# Towards Quantum Computation with Ultracold Fermi Atoms

## Yanay Florshaim

# Acknowledgments

First and foremost, I would like to thank my supervisor, Prof. Yoav Sagi, for his great support in every aspect of my M.Sc. Yoav's contagious enthusiasm for research and his vast knowledge are all a student can hope for from a supervisor. To work in a new lab is not an easy task, with many difficulties and mistakes along the way, but due to Yoav's optimistic vision and will to teach and share his wisdom, things always turned out for the best.

I would like to thank Dr. Andrey Gandman ,our research associate, for his help in experimental issues. In addition, I would like to thanks Dr. Jonathan Nemirovsky for his theoretical work including numerical simulation and calculation.

I would like to thank all my current lab colleagues: Kostya Sekadorov, Iris Eitan and Gal Ness. Since many of work was done in collaboration with you, I want to thank you for the professional help and good advice.

I'd like to thank my parents for their support and encouragement during my studies.

Finally I want to thank my wife Sara and my daughters Arbel, Be'eri and Yahav for their love, support and assistance during my studies.

# Contents

# 1 Introduction

In quantum mechanics, the dimension of the Hilbert space grows exponentially with the system size. In order to represent a quantum state with $n$ particles in classical computation we need an order of $C^n$ bits, where $C$ is a constant. Therefore, the possibility of making a calculation of many-body quantum states in classical computing becomes practically impossible. To overcome this problem, it was first proposed by Richard Feynman [1] to use a quantum computational machine ("Quantum Computer"). A quantum computer is able to calculate not only simulation of quantum dynamics but also solve complex mathematical problems. In addition, quantum computer is much faster than classical one in a factorial problems[2] and in database searching [3]. For two decades, researchers have been trying to implement quantum computation using different platforms but, all these platforms are suffer from inherent experimentally limits [4, 5, 6, 7, 8, 9]. Here we present a new platform of a quantum computer system with ultracold fermionic atoms. We take advantage of the fermionic statistics and ultracold atom system benefits (Feshbach resonance and the ability to capture single atoms in optical traps) in order to carry out a new protocol for quantum gate operators.

Quantum computer system requirements as stated by D.DiVincenzo [10] should comply with 5 conditions:.

- **Quantum state.** The quantum state encapsulates the quantum information in a quantum computer.The state is usually spanned by two basis vector ,$|0\rangle$ and $|1\rangle$, and the qubit state is defined by

$$|\psi\rangle = \alpha |0\rangle + \beta |1\rangle$$

  where $\alpha$ and $\beta$ are complex numbers. When the qubit is measured, with the probability of $|\alpha|^2$ it will be in a state $|0\rangle$ and with a probability of $|\beta|^2$ in a state $|1\rangle$, satisfying the relation:

$$|\alpha|^2 + |\beta|^2 = 1$$

  since the probabilities must sum to one.

- **Preparation of the Initial State.** One should be able to prepare the initial state of the qubit. The particular initial state is of little importance as we can transform it to any other state using several quantum gates. However, it is important that the initial state will be created with high fidelity.

- **Quantum gates.** In order to preform any quantum calculation we need several unitary operations ("Quantum Gates") which form a universal set, namely any other operation can be decoposed to a series of gate operations taken from this set. The quantum gates operate on one or two qubit. Examples of one qubit gates include the Hadamard gate, the phase gate and the $\pi/8$ gate. The two qubit gate is C-NOT. In place of a C-NOT gate it is also possible to use a $\sqrt{SWAP}$ gate [11].

1. **Hadamard gate**. The Hadamard gate is a one qubit rotation. This gate maps the qubit states $|0\rangle$ and $|1\rangle$ to two superpositions with equal weight.

$$U = \frac{|0\rangle + |1\rangle}{\sqrt{2}}\langle 0| + \frac{|0\rangle - |1\rangle}{\sqrt{2}}\langle 1|$$

or in a matrix representation

$$U = \frac{1}{\sqrt{2}}\begin{bmatrix} 1 & 1 \\ 1 & -1 \end{bmatrix}$$

It is worth noting here that hadamard gate is essentially a "beam splitter" for the two "modes" $|0\rangle$ and $|1\rangle$, namely $|0\rangle \rightarrow \frac{|0\rangle + |1\rangle}{\sqrt{2}}$ and $|1\rangle \rightarrow \frac{|0\rangle - |1\rangle}{\sqrt{2}}$.

2. **Phase gate.** The phase gate is a one qubit gate that leaves the basis $|0\rangle$ without a change while transforming $|1\rangle \rightarrow e^{i\phi}|1\rangle$.

$$U = |0\rangle\langle 0| + e^{i\phi}|1\rangle\langle 1|$$

or in a matrix representation

$$U_\phi = \begin{bmatrix} 1 & 0 \\ 0 & e^{i\phi} \end{bmatrix}$$

Where $\phi$ is the *phase shift*. Some common examples are the phase gate with $\phi = \pi/2$ , the $\pi/8$ gate with $\phi = \pi/4$ and the Pauli-Z gate with $\phi = \pi$.

3. $\underline{\sqrt{SWAP}}$ **gate**. A $\sqrt{SWAP}$ gate is operated on the mixed states and swap them in half way. It is defined by

$$U_{\sqrt{swap}} = \begin{bmatrix} 1 & 0 & 0 & 0 \\ 0 & \frac{1}{2}(1+i) & \frac{1}{2}(1-i) & 0 \\ 0 & \frac{1}{2}(1-i) & \frac{1}{2}(1+i) & 0 \\ 0 & 0 & 0 & 1 \end{bmatrix} \tag{1}$$

with respect to the basis $|00\rangle$, $|01\rangle$, $|10\rangle$, $|11\rangle$.

By using all these gates we can reduce any unitary operation of $n$ qubits to a cumulative series of these gates [12].

- **Ability to Measure the Result.** The ability to measure the final state of the system is required for all computation schemes.

- **Scalability.** All physical resources (space, money, nunber of components, etc.) should not scale as $X^n$, where $X$ is some constant and $n$ is the number of qubits. This requirement ensures the system is technically feasible.

In quantum the phase between states are determinate and the system is coherent. However, in the real world, a quantum computer is not completely isolated and the coherence decay with time $T_D$ (decoherence time) . It is imperative that the decoherence time is much longer than the gate operation

timescale $T_{gate}$ times the typical number of operation $N$.

$$\frac{N \cdot T_{gate}}{T_I} \ll 1$$

To date, attempts have been made to use different physical systems to meet these requirements and realize a quantum computer. For example, in an optical system the polarization of a photon is taken as a state and optical component, such as polarizing beam splitters and a wavelength plates are used to manipulate the state. Optical systems suffer from the fact that photon do not interact and therefore it is quite difficult to implement two qubit gates [6]. Another platform of quantum calculations is ion traps [4, 5]. Here one uses the internal state of the ion as the qubit and quantum gates are implemented using the coupling of the ions to lasers. These systems are probably the closest to date to a successful implementation, but there are still unsolved issues with the scalability and heating from the electrodes. Another platform that was investigated is based on localized electron spins as qubits in quantum dots [8] the interaction between the spins can realize the quantum gates. The interaction and the detection are done using laser. The main problem in this platform is the strong coupling of the qubit to a noisy bath (i.e. phonons) which this limits the ratio of operation time (10 psec) to decoherence gate operation time (1 nsec). Another platform that could theoretically serve to perform quantum computation is neutral atoms in a 1D optical lattice [7].In this method, they used two sub-level $(m_f)$ in the ground state of an optical lattice and described a one qubit gate with Raman sidebant transition $\left(t_{\pi/2} \sim 150 \, nsec\right)$ and with RF pulse $\left(t_{\pi/2} \sim 30 \, \mu sec\right)$. In addition, they use a movable optical tweezer for the two qubits gate to transport qubit to another one .

In this thesis we present a new platform of quantum computation which is based on fermionic atoms in an optical microtrap. The basis for this platform is the fermionic statistic of the qubits. In addition, with ultracold atoms we can control the interaction between atoms by using Feshbach resonance. Furthermore, the depth of the micro-trap, shape and position can be controlled dynamically.

4

In recent years there has been substantial experimental progress with preparation and measurement of an individual atoms in the ground state of an optical microtrap [13, 14]. Several techniques have been used to accomplish this:.

1. Light-Assisted Collisions (LAC) can reduce the number of atoms by shining the atoms with a near resonant laser. By carefully tuning the frequency, it is possible to increases the probability that one of the atoms will leave the trap while the other will stay. atoms one by one by intensifying their interaction. [15]. After the LAC has been used to remove all atoms other than one, it is possible to use Raman side-band cooling technique to cool this single atoms to the ground state of the trap [16].

2. Loading spin polarized atoms to a microtrap with one state or several atoms to a low optical microtrap (with several states) and then by creating a linear potential that removes all bound states other than one it is possible to end up with only a single atom. remaining with one state[17].

The measurement of a single fermion $^{40}K$ atom in a trap is clearly not a simple task. In this field there are few studies which succeeded in doing so [13, 14, 16]. In these studies, a sideband cooling technique was employed in order to cool the atoms and at the same time to measure them fluorescence.

Our platform is based on ultracold fermion $\left(^{40}K\right)$ neutral atoms trapped in an optical micro-trap. There still remain some open questions regarding the experimental system which I will elaborate on.. In chapter 2, I present the theory behind our proposed scheme. In chapter 3, I give some relevant ultracold atom background. In chapter 4, I present the experimental work done en route to implementing the new computation scheme.

# 2 New platform of quantum computation

In this chapter I explain how we fulfill the five principles mentioned in the introduction. The $\sqrt{SWAP}$ gate was developed by Dr. Jonathan Nemirovsky. I performed the numerical simulations with a code that was also developed by Dr. Nemirovsky.

## 2.1 The new scheme

### 2.1.1 The Qubit

Our quantum computer is based on two internal energy levels of an single atom in microtrap. We choose $|0\rangle = |9/2, -9/2\rangle$ and $|1\rangle = |9/2, -7/2\rangle$ with notation $|f, m_f\rangle$ where $f$ is the total atomic spin and $m_f$ is the projection in z direction (set by external magnetic field). We can choose any two $m_f$ states but we want to control the interaction between the atoms by means of a Feshbach resonance. The Feshbach resonance between $m_f = -9/2$ and $m_f = -7/2$ is at $B = 202.2\ G$ [18]. We can also work in a spin state $|0\rangle = |9/2, -9/2\rangle$ and $|1\rangle = |9/2, -5/2\rangle$ or $|0\rangle = |9/2, -7/2\rangle$ and $|1\rangle = |9/2, -5/2\rangle$. Their Feshbach resonance is $B_{-\frac{9}{2}, -\frac{5}{2}} = 224.21\ G$ and $B_{-\frac{7}{2}, -\frac{5}{2}} = 174\ G$ [18]. However, with these states there is a possibility of spin exchange collisions which means the qubit can leave the designated Hilbert space.

### 2.1.2 Preparation of the Initial State

In our method initial state requires a single atom state in each qubit. As I mentioned above, the preparation of one atom in a microtrap can be done in two ways.

The first method ("Fast approach") is based on loading several atoms ($\sim 10 - 20$) from a 3D Mgneto-Optical-Trap directly to an optical microtrap and with a LAC [15] with a blue detune laser from the $D_1$ transition reducing the atom's number to one (this study has been carried with bosonic $^{85}Rb$). When will trap contain a single atom, we can cool the atom to the ground state with Raman sideband cooling [16]. This process gives us two more features. We can measure the fluorescence and calculate the atom number at the optical microtrap (zero, one or more). Additionally, we can know which qubit is empty and do not use its for the quantum calculation.

The second way ("Degenerate fermi gas") is to reduce the trap depth until there is only a single bound

state left [17]. In ref [17] it was shown that by using a gradient of magnetic field they controlled the number of atoms (up to single atom trapped $\left(^{6}Li\right)$). In order to get high occupation probability of lowest state due to Fermi-Dirac statistics, such an experiment must begin at very low temperatures $T/T_f < 0.5$ ,In other words, $T \sim 40nK$. The time it takes to prepare atoms at this temperature is about 80 seconds.

In table 1 we compare these two system. The advantages of the fast approach are rapid data acquisition and it is experimentally simpler, but the disadvantages may be higher final temperature of the captured atom. Also, there are many unknowns with this method which still need to be investigated before we will be able to conclude this approach is viable. The advantages of the degenerate fermi gas is low final temperature of the trapped atom, but the disadvantage is long preparation time (~80 sec ). In chapter 4 I present the two systems in more detail.

|  | Fast approach | Degenerate fermi gas |
|---|---|---|
| Number of Vacuum Cell | One or Two | Two or Three |
| 2D and 3D MOT (15-40 sec) | maybe just 3D | ✓ |
| $D_1$cooling (20 msec) | ✓ | ✓ |
| Magnetic Trap & RF Evaporation (30 sec) | X | ✓ |
| Optic or Magnetic Transfer (1-3 sec) | X | ✓ |
| Optic Evaporation | X | ✓ |
| Sideband Cooling (2 sec) | ✓ | X |

Table 1: A comparison between the two systems. As shown in the Table the preferable system in terms of time is the one using Light-Assisted Collisions. However, we are unsure if these will succeed.

### 2.1.3 Quantum gates

After preparing one or two qubits made of single atoms, we need to be able to preform quantum gate operation. In order to call our system "Quantum Computer" ,as I explained in paragraph one, we need to adapt the Hadamard gate, the phase gate,$\pi/8$ gate and the $\sqrt{SWAP}$ gate to our system.

**Single qubit gates**    An arbitrary single qubit state can be written

$$|\psi\rangle = e^{i\gamma}\left(\cos\frac{\theta}{2}\,|0\rangle + e^{i\phi}\sin\frac{\theta}{2}\,|1\rangle\right)$$
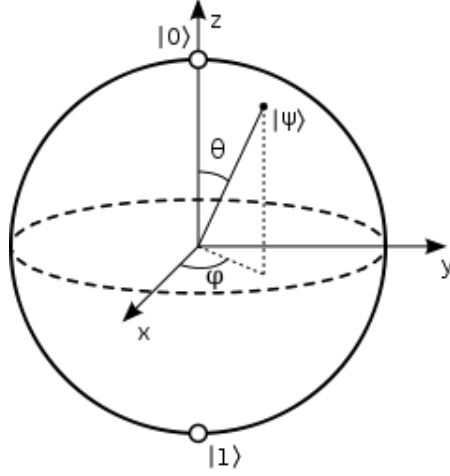
Figure 1: *Bloch sphere*

where $\theta$, $\phi$ and $\gamma$ are real numbers. The numbers $0 \leq \theta \leq \pi$ and $0 \leq \phi \leq 2\pi$ define a point on a unit three-dimensional sphere ,commonly called, the *Bloch sphere*. A qubit state with an arbitrary value of $\gamma$ is represented by point on the Bloch sphere as the factor of $e^{i\gamma}$ has no observable effects. we can then write:

$$|\psi\rangle = \cos\frac{\theta}{2}|0\rangle + e^{i\phi}\sin\frac{\theta}{2}|1\rangle$$

The Bloch sphere is $S^2$ which can be embedded in $\mathbb{R}^3$ using the following map

$$f : (r = 1, \phi, \theta) \rightarrow (\cos\phi\sin\theta, \sin\phi\sin\theta, \cos\theta)$$

The rotations of Bloch vectors can be generated by Pauli matrices $\hat{\sigma_x} = \begin{pmatrix} 0 & 1 \\ 1 & 0 \end{pmatrix}$, $\hat{\sigma_y} = \begin{pmatrix} 0 & -i \\ i & 0 \end{pmatrix}$

and $\hat{\sigma}_z = \begin{pmatrix} 1 & 0 \\ 0 & -1 \end{pmatrix}$. Therefore, the rotation around the axes is given by

$$R_x\left(\theta\right) \equiv e^{-i\frac{\theta}{2}\cdot\hat{\sigma}_x} = \cos\frac{\theta}{2}\hat{\mathbb{I}} - i\sin\frac{\theta}{2}\hat{\sigma}_x = \begin{bmatrix} \cos\frac{\theta}{2} & -i\sin\frac{\theta}{2} \\ -i\sin\frac{\theta}{2} & \cos\frac{\theta}{2} \end{bmatrix}$$

$$R_y\left(\theta\right) \equiv e^{-i\frac{\theta}{2}\cdot\hat{\sigma}_y} = \cos\frac{\theta}{2}\hat{\mathbb{I}} - i\sin\frac{\theta}{2}\hat{\sigma}_y = \begin{bmatrix} \cos\frac{\theta}{2} & -\sin\frac{\theta}{2} \\ -\sin\frac{\theta}{2} & \cos\frac{\theta}{2} \end{bmatrix}$$

$$R_z\left(\theta\right) \equiv e^{-i\frac{\theta}{2}\cdot\hat{\sigma}_z} = \cos\frac{\theta}{2}\hat{\mathbb{I}} - i\sin\frac{\theta}{2}\hat{\sigma}_z = \begin{bmatrix} \exp\left(-i\frac{\theta}{2}\right) & 0 \\ 0 & \exp\left(i\frac{\theta}{2}\right) \end{bmatrix}$$

Any unitary transformation on a single qubit can be decomposed into a rotation in the Bloch sphere around some axis $\hat{n}$ by an angle $\theta$, multiplied by a global phase $\phi$

$$U = e^{i\phi}R_{\hat{n}}\left(\theta\right)$$

Next, we define the single qubit gates using these terms.

- **Hadamard gate.** A Hadamard gate operator can be represented by rotations around the $\hat{x}$ and $\hat{z}$ axes. We choose $\theta = \pi/2$, $\phi = \pi/2$ and $\hat{n} = (1, 0, 1)/\sqrt{2}$

$$U_{\text{hadamard}} = e^{i\frac{\pi}{2}}R_{\hat{n}}\left(\pi\right)$$
$$= i\left[\cos\frac{\pi}{2}\hat{\mathbb{I}} - i\sin\frac{\pi}{2}\left(\frac{\hat{\sigma}_x + \hat{\sigma}_z}{\sqrt{2}}\right)\right]$$
$$= \frac{1}{\sqrt{2}}\begin{bmatrix} 1 & 1 \\ 1 & -1 \end{bmatrix}$$

- **Phase gate.** A Phase Gate Operator can be represented by taking $\theta = \pi/2$ , $\phi = \pi/4$ and

9

$$\hat{n} = (0,0,1)$$

$$U_{\pi/2} = e^{i\frac{\pi}{4}} R_z \left(\frac{\pi}{2}\right) = e^{i\frac{\pi}{4}} \begin{bmatrix} \exp\left(-i\frac{\pi}{4}\right) & 0 \\ 0 & \exp\left(i\frac{\pi}{4}\right) \end{bmatrix} = \begin{bmatrix} 1 & 0 \\ 0 & \exp\left(i\frac{\pi}{2}\right) \end{bmatrix}$$

$$U_{\pi/2} = \begin{bmatrix} 1 & 0 \\ 0 & i \end{bmatrix}$$

- **$\pi/8$ Gate.** A $\pi/8$ Gate Operator can be represented by using $\theta = \pi/4$, $\phi = \pi/8$ and $\hat{n} = (0,0,1)$

$$U_{\frac{\pi}{8}} = e^{i\frac{\pi}{8}} R_z \left(\frac{\pi}{4}\right) = e^{i\frac{\pi}{8}} \begin{bmatrix} \exp\left(-i\frac{\pi}{8}\right) & 0 \\ 0 & \exp\left(i\frac{\pi}{8}\right) \end{bmatrix} = \begin{bmatrix} 1 & 0 \\ 0 & \exp\left(i\frac{\pi}{4}\right) \end{bmatrix}$$

We can realize these gates in our system, by coupling a two level system to an external EM field [19, 20]. Let us write the state of the atom as

$$\psi(t) = C_0(t)\,|\psi_0\rangle + C_1(t)\,|\psi_1\rangle$$

where $|\psi_n\rangle$ are the energy eignestates of the atoms which are relevant to the computational scheme, $C_0(t) = e^{-E_n t/\hbar} C_0(0)$ are the complex amplitude and $E_n = \hbar\omega_n$ are the eigenvalue. we write the Hamiltonian as

$$H = H_0 + V(t)$$

where $H_0$ is the free Hamiltonian and $V(t)$ the interaction between the electromagnetic field and the atom.

$$V(t) = \mu\left[A(t)\,e^{-i\omega t} + A^*(t)\,e^{i\omega t}\right]$$

where $\mu$ is the electric or magnetic moment, $\omega$ is the EM field frequency and $A(t)$ represents the EM

field amplitude, which we can treat classically. We calculate the matrix element $\langle \psi_n | V(t) | \psi_m \rangle$

$$V(t) = \begin{bmatrix} 0 & V_{0,1} \\ V_{1,0} & 0 \end{bmatrix}$$

where $V_{n,m} = -\mu_{n,m}\delta_{n,m} \left[ A(t) e^{-i\omega t} + A^*(t) e^{i\omega t} \right]$. Therefore, the Hamiltonian is

$$H = \begin{bmatrix} E_0 & V_{0,1} \\ V_{1,0} & E_1 \end{bmatrix}$$

The time-dependent Schrodinger equation for the two-level system is

$$i\hbar \frac{\partial \psi}{\partial t} = H\psi$$

$$i\frac{d}{dt}\begin{pmatrix} B_0(t) \\ B_1(t) \end{pmatrix} = \begin{pmatrix} \omega_0 & V_{0,1}/\hbar \\ V_{1,0}/\hbar & \omega_1 \end{pmatrix} \begin{pmatrix} B_0(t) \\ B_1(t) \end{pmatrix}$$

by transform the amplitudes $B_i(t) = C_i(t) e^{-\omega_i t}$ we can get

$$i\hbar\frac{d}{dt}\begin{pmatrix} C_0(t) \\ C_1(t) \end{pmatrix} = \begin{pmatrix} 0 & -\mu \left[ A(t) e^{-i\omega t} + A^*(t) e^{i\omega t} \right] e^{-i\omega_{10}t} \\ -\mu \left[ A(t) e^{-i\omega t} + A^*(t) e^{i\omega t} \right] e^{-i\omega_{10}t} & 0 \end{pmatrix} \begin{pmatrix} C_0(t) \\ C_1(t) \end{pmatrix}$$

where $\omega_{10} = \omega_1 - \omega_0$ . In the rotating wave approximation ,the term that oscillate quickly are dropped and the term that rotate slowly remains.

$$i\hbar\frac{d}{dt}\begin{pmatrix} C_0(t) \\ C_1(t) \end{pmatrix} = \begin{pmatrix} 0 & \frac{\Omega^*}{2} e^{-i\delta t} \\ \frac{\Omega}{2} e^{-i\delta t} & 0 \end{pmatrix} \begin{pmatrix} C_0(t) \\ C_1(t) \end{pmatrix}$$

where $\delta = \omega - \omega_{01}$ is the detuning of the EM field from resonance and $\Omega = 2\mu A/\hbar$ is the Rabi frequency.

In the resonant case, the evolution of Bloch vector in the presence of an external pulse (Rabi pulse)

can be described [20]

$$u(t) = \begin{pmatrix} 1 & 0 & 0 \\ 0 & \cos\theta(t) & \sin\theta(t) \\ 0 & -\sin\theta(t) & \cos\theta(t) \end{pmatrix} u_0$$

where $\theta(t) = \int_0^t \sqrt{|\Omega(t')|^2 + \delta^2} dt'$. Namley the Rabi pulse rotates the Bloch vector about the x axis. In the state vector representation, a resonant pulse of duration t is expressed by the application of a unitary operator $U(t)$ to the state vector:

$$|\psi(t)\rangle = \hat{U}(t) |\psi_0\rangle$$

$$\hat{U}(t) = \begin{pmatrix} \cos\frac{\theta(t)}{2} & i\sin\frac{\theta(t)}{2} \\ -i\sin\frac{\theta(t)}{2} & \cos\frac{\theta(t)}{2} \end{pmatrix} \tag{2}$$

by set the angle $\theta(t)$ we can get the one qubit gate. This can be done with a coils that preform a magnetic feild with $\omega_1$ and, in this case, the Rabi frequency is given by $\Omega = \mu B/\hbar$ and the detuning is $\delta = \omega_1 - \omega_0$.

For example, by taking EM pulse with $\theta(t) = \pi/2$

$$\hat{U(t)}_{\pi/2} = \frac{1}{\sqrt{2}} \begin{pmatrix} 1 & i \\ -i & 1 \end{pmatrix}$$

If the atom is initially prepared in one of the basis state, a $\pi/2$ pulse transform it into a superposition state

$$|0\rangle \rightarrow \frac{1}{\sqrt{2}} (|0\rangle + i|1\rangle) \qquad |1\rangle \rightarrow \frac{1}{\sqrt{2}}(|1\rangle - i|0\rangle)$$

Therefore by taking RF pulse with detuning relevant to $|0\rangle$ or $|1\rangle$ we can drive the atom state with Phase gate, $\pi/4$ gate and hadamard gate.

**Two Qubit gate** In order to implement the two qubit $\sqrt{SWAP}$ gate we are going to utilize two unique advantages of ultracold atoms.

- Ability to control the interaction between atoms around Feshbach resonance [21].

- Ability to shape the potential landscape using far off resonance light, and thus control the atom tunneling between two traps [17].

These, together with fermionic statistics, are the basis for a new protocol for $\sqrt{SWAP}$ gate. This protocol is original, but similar in some aspects to the gate first describe in ref.[22] .We consider two optical microtraps with one atom at each site, with a distance $d$ between them. Using second quantization and the Fermi-Hubbard model [23], the Hamiltonian is given by

$$H_{J,U} = J \left( \hat{u_1}^\dagger \hat{u_2} + \hat{u_2}^\dagger \hat{u_1} + \hat{d_1}^\dagger \hat{d_2} + \hat{d_2}^\dagger \hat{d_1} \right) + 2U \left( \hat{u_1}^\dagger \hat{u_1} \hat{d_1}^\dagger \hat{d_1} + \hat{u_2}^\dagger \hat{u_2} \hat{d_2}^\dagger \hat{d_2} \right)$$

$$\equiv J \cdot H_J + U \cdot H_u$$

Where $J$ is the tunneling energy, $U$ is on site interaction energy, $\hat{u_i}$ and $\hat{u_i}^\dagger$ are annihilation and creation operators of particle $i$ in state "up", i.e. $|1\rangle$, $\hat{d_i}$ and $\hat{d_i}^\dagger$ are annihilation and creation operators of particle $i$ in state "down", i.e. $|0\rangle$ with the usual fermionic commutation relations [24]. We assume only on site interactions because of the short range interaction atoms e.g. $^{40}K$.

Firstly, I explain the operation of the $\sqrt{SWAP}$ gate in three steps. At each step the Hamiltonian is time independent and the unitary evolution operator has the form

$$\hat{U} = e^{\frac{-i}{\hbar} H \cdot t}$$

The $\sqrt{SWAP}$ gate can be divided into

$$\hat{U}_{\sqrt{SWAP}} = e^{-\frac{i}{\hbar} J \cdot H_J \cdot t_1} e^{-\frac{i}{\hbar} U \cdot H_u \cdot t_2} e^{-\frac{i}{\hbar} J \cdot H_J \cdot t_1} \tag{3}$$

13

where $t_1 = \frac{\pi\hbar}{4J}$ and $t_2 = \frac{\pi\hbar}{4U}$. To prove it, we need to calculate the time evolution of $H_J$ and $H_U$. For $H_J$ we note that

$$H_J\left(\hat{d_1}^\dagger \hat{u_2}^\dagger + \hat{d_2}^\dagger \hat{u_1}^\dagger\right)|0\rangle = 2\left(\hat{d_1}^\dagger \hat{u_1}^\dagger + \hat{d_2}^\dagger \hat{u_2}^\dagger\right)|0\rangle \tag{4}$$
$$H_J\left(\hat{d_1}^\dagger \hat{u_1}^\dagger + \hat{d_2}^\dagger \hat{u_2}^\dagger\right)|0\rangle = 2\left(\hat{d_1}^\dagger \hat{u_2}^\dagger + \hat{d_2}^\dagger \hat{u_1}^\dagger\right)|0\rangle$$

$$H_J\left(\hat{d_1}^\dagger \hat{u_2}^\dagger - \hat{d_2}^\dagger \hat{u_1}^\dagger\right)|0\rangle = 0$$
$$H_J\left(\hat{u_1}^\dagger \hat{u_2}^\dagger\right)|0\rangle = 0 \tag{5}$$
$$H_J\left(\hat{d_1}^\dagger \hat{d_2}^\dagger\right)|0\rangle = 0$$

Now we look at equations (4), and get a simple matrix

$$i\frac{d}{dt}\begin{bmatrix} A_1(t) \\ A_2(t) \end{bmatrix} = \begin{bmatrix} 0 & 2 \\ 2 & 0 \end{bmatrix}\begin{bmatrix} A_1(t) \\ A_2(t) \end{bmatrix} \tag{6}$$

Where $A_1(t)$ and $A_2(t)$ are time dependent states amplitude, i.e. $\begin{bmatrix} |0\rangle \\ |1\rangle \end{bmatrix}$. The solutions to eq.6 are:

$$A_1(t) = A\cos\left(2\left(t-t_0\right)\right) \qquad A_2(t) = A\sin\left(2\left(t-t_0\right)\right)$$

Now we add the solution of equations eq.5(homogeneous solution), and we get that the general solution is

$$|\psi\rangle = (C_{00}\hat{d_1}^\dagger \hat{d_2}^\dagger + C_{11}\hat{u_1}^\dagger \hat{u_2}^\dagger + C_{12}\left(\hat{d_1}^\dagger \hat{u_2}^\dagger - \hat{d_2}^\dagger \hat{u_1}^\dagger\right) +$$
$$+ A_{12}\left[\cos\left(2\left(t-t_0\right)\right)\left(\hat{d_1}^\dagger \hat{u_2}^\dagger - \hat{d_2}^\dagger \hat{u_1}^\dagger\right) - i\sin\left(2\left(t-t_0\right)\right)\left(\hat{d_1}^\dagger \hat{u_1}^\dagger + \hat{d_2}^\dagger \hat{u_2}^\dagger\right)\right]|0\rangle$$

14

Where $|\psi\rangle$ is a solution to the time evolution equation $i\frac{d}{dt}|\psi\rangle = H_J |\psi\rangle$. Now we can choose, $C_{11} = C_{12} = C_{00} = 0$ and $t_0 = 0$ . This means that the singlet $\hat{d_1}^\dagger \hat{u_2}^\dagger + \hat{d_2}^\dagger \hat{u_1}^\dagger = \hat{d_1}^\dagger \hat{u_2}^\dagger - \hat{u_1}^\dagger \hat{d_2}^\dagger$ after $t_1 = \frac{\pi\hbar}{4J}$ into

$$e^{-i\frac{\pi}{4}H_J} \to -i\left(\hat{d_1}^\dagger \hat{u_1}^\dagger + \hat{d_2}^\dagger \hat{u_2}^\dagger\right).$$

Now we find the solution for $H_U$ .

$$H_u\left(\hat{d_1}^\dagger \hat{u_1}^\dagger + \hat{d_2}^\dagger \hat{u_2}^\dagger\right)|0\rangle = 2\left(\hat{d_1}^\dagger \hat{u_1}^\dagger + \hat{d_2}^\dagger \hat{u_2}^\dagger\right)|0\rangle$$

$$H_u\left(\hat{u_2}^\dagger \hat{u_1}^\dagger\right)|0\rangle = 0 \qquad H_u\left(\hat{d_2}^\dagger \hat{u_1}^\dagger\right)|0\rangle = 0$$

$$H_u\left(\hat{d_1}^\dagger \hat{u_2}^\dagger\right)|0\rangle = 0 \qquad H_u\left(\hat{d_2}^\dagger \hat{d_1}^\dagger\right)|0\rangle = 0$$

Here the solution is simple all the single particle states are stationary while the solution for the state $|\psi_0\rangle = \left(\hat{d_1}^\dagger \hat{u_1}^\dagger + \hat{d_2}^\dagger \hat{u_2}^\dagger\right)$ reads

$$|\psi_+\rangle = e^{2it}|\psi_0\rangle \tag{7}$$

Now we can calculate eq.(3) . The first term with $t = t_1$ is

$$|0_1\rangle = e^{-\frac{i\pi}{4}H_J}|0_{initial}\rangle$$

We can see that due to the Pauli principle, all the three symmetric states $\hat{d_1}^\dagger \hat{u_2}^\dagger$ , $\hat{u_2}^\dagger \hat{u_1}^\dagger$, $\left(\hat{d_1}^\dagger \hat{u_2}^\dagger + \hat{d_2}^\dagger \hat{u_1}^\dagger\right)$ are stationary in time eq.(5). The singlet state, which is anti-symmetric evolves as follows $\hat{d_1}^\dagger \hat{u_2}^\dagger - \hat{u_1}^\dagger \hat{d_2}^\dagger \xrightarrow{H_J} \hat{d_1}^\dagger \hat{u_2}^\dagger + \hat{d_2}^\dagger \hat{u_1}^\dagger$. Therefore, at the end of the first evolution, the symmetric states are unchanged while the anti-symmetric state becames a state of "two particle" (i.e. doublon $-i\left(\hat{d_1}^\dagger \hat{u_1}^\dagger + \hat{d_2}^\dagger \hat{u_2}^\dagger\right)$) .The second evolution with $t = t_2$ (duo to eq. 7)

$$|0_2\rangle = e^{-\frac{i}{\hbar}U\cdot H_u \cdot t_2}|0_1\rangle$$

the "two particle" state get a phase of $e^{-i\pi/2} = -i$ , and transforms it into $-\left(\hat{d_1}^\dagger \hat{u_1}^\dagger + \hat{d_2}^\dagger \hat{u_2}^\dagger\right)$ .The three symmetric states does not change. Finally, by repeating the first evolution with $t = t_1$, the

15

symmetric states are unchanged and the "doublon" state gets a phase of $-i$. Now it reverts back to an anti-symmetric singlet state

$$\left(\hat{d_1}^\dagger \hat{u_2}^\dagger - \hat{d_2}^\dagger \hat{u_1}^\dagger\right) \overset{\sqrt{SWAP}}{\to} i\left(\hat{d_1}^\dagger \hat{u_2}^\dagger - \hat{d_2}^\dagger \hat{u_1}^\dagger\right)$$

In conclusion, all the three steps give us

- $\hat{d_1}^\dagger \hat{d_2}^\dagger \to \hat{d_1}^\dagger \hat{d_2}^\dagger$

- $\hat{u_1}^\dagger \hat{u_2}^\dagger \to \hat{u_1}^\dagger \hat{u_2}^\dagger$

- $\hat{d_1}^\dagger \hat{u_2}^\dagger + \hat{d_2}^\dagger \hat{u_1}^\dagger \to \hat{d_1}^\dagger \hat{u_2}^\dagger + \hat{d_2}^\dagger \hat{u_1}^\dagger$

- $\hat{d_1}^\dagger \hat{u_2}^\dagger - \hat{d_2}^\dagger \hat{u_1}^\dagger \to i\left(\hat{d_1}^\dagger \hat{u_2}^\dagger - \hat{d_2}^\dagger \hat{u_1}^\dagger\right)$

Therefore, all these three actions together are equivalent to a $\sqrt{SWAP}$ gate. In matrix notation,

- $\hat{d_1}^\dagger \hat{d_2}^\dagger \to \hat{d_1}^\dagger \hat{d_2}^\dagger$

- $\hat{u_1}^\dagger \hat{u_2}^\dagger \to \hat{u_1}^\dagger \hat{u_2}^\dagger$

- $\hat{d_1}^\dagger \hat{u_2}^\dagger = \frac{1}{2}\left(\hat{d_1}^\dagger \hat{u_2}^\dagger + \hat{d_2}^\dagger \hat{u_1}^\dagger + \hat{d_1}^\dagger \hat{u_2}^\dagger - \hat{d_2}^\dagger \hat{u_1}^\dagger\right) \to$
  $\frac{1}{2}\left(\hat{d_1}^\dagger \hat{u_2}^\dagger + \hat{d_2}^\dagger \hat{u_1}^\dagger + i\left(\hat{d_1}^\dagger \hat{u_2}^\dagger - \hat{d_2}^\dagger \hat{u_1}^\dagger\right)\right) = \frac{1+i}{2}\hat{d_1}^\dagger \hat{u_2}^\dagger + \frac{1-i}{2}\hat{d_2}^\dagger \hat{u_1}^\dagger$

- $\hat{d_2}^\dagger \hat{u_1}^\dagger = \frac{1}{2}\left(\hat{d_1}^\dagger \hat{u_2}^\dagger + \hat{d_2}^\dagger \hat{u_1}^\dagger - \hat{d_1}^\dagger \hat{u_2}^\dagger - \hat{d_2}^\dagger \hat{u_1}^\dagger\right) \to$
  $\frac{1}{2}\left(\hat{d_1}^\dagger \hat{u_2}^\dagger + \hat{d_2}^\dagger \hat{u_1}^\dagger - i\left(\hat{d_1}^\dagger \hat{u_2}^\dagger - \hat{d_2}^\dagger \hat{u_1}^\dagger\right)\right) = \frac{1-i}{2}\hat{d_1}^\dagger \hat{u_2}^\dagger + \frac{1+i}{2}\hat{d_2}^\dagger \hat{u_1}^\dagger$

which is the same as the matrix form that I showed above in ,eq.(1)

We can simplify the gate farther to be accomplished in two or even one step. We note that

$$H_{J,U}\left(\hat{d_1}^\dagger \hat{u_2}^\dagger + \hat{d_2}^\dagger \hat{u_1}^\dagger\right)|0\rangle = 2J\left(\hat{d_1}^\dagger \hat{u_1}^\dagger + \hat{d_2}^\dagger \hat{u_2}^\dagger\right)|0\rangle$$
$$H_{J,U}\left(\hat{d_1}^\dagger \hat{u_1}^\dagger + \hat{d_2}^\dagger \hat{u_2}^\dagger\right)|0\rangle = 2J\left(\hat{d_1}^\dagger \hat{u_2}^\dagger + \hat{d_2}^\dagger \hat{u_1}^\dagger\right)|0\rangle + U\left(\hat{d_1}^\dagger \hat{u_1}^\dagger + \hat{d_2}^\dagger \hat{u_2}^\dagger\right)|0\rangle$$

Now we can write these in a matrix form for the anti-symmetric state

$$
i\frac{d}{dt}\begin{bmatrix} A_1\left(t\right) \\ A_2\left(t\right) \end{bmatrix} = \begin{bmatrix} 0 & 2J \\ 2J & 2U \end{bmatrix}\begin{bmatrix} A_1\left(t\right) \\ A_2\left(t\right) \end{bmatrix} \tag{8}
$$

Where the matrix eigenvalues are

$$
\lambda_{1,2} = U \pm \sqrt{4J^2 + U^2}
$$

and the eigenvectors are:

$$
V_{1,2} = \frac{1}{2J}\begin{bmatrix} -\lambda_{2,1} \\ 2J \end{bmatrix}
$$

So, the solution is given by $Ae^{-i\lambda_1 t}V_1 + Be^{-i\lambda_2 t}V_2$ and $AV_1 + BV_2 = \begin{bmatrix} 1 \\ 0 \end{bmatrix}$. The second term solution is $A = -B$. Therefore, the solution for the amplitude ,eq. (8), is

$$
= \frac{Ae^{-iUt}}{2J}\left( e^{-it\sqrt{4J^2+U^2}}\begin{bmatrix} -U + \sqrt{4J^2+U^2} \\ 2J \end{bmatrix} - e^{it\sqrt{4J^2+U^2}}\begin{bmatrix} -U - \sqrt{4J^2+U^2} \\ 2J \end{bmatrix} \right) =
$$

$$
= Ae^{-iUt}\begin{bmatrix} \frac{\sqrt{4J^2+U^2}}{J}\cos\left(t\sqrt{4J^2+U^2}\right) + i\frac{U}{J}\sin\left(t\sqrt{4J^2+U^2}\right) \\ -2i\sin\left(t\sqrt{4J^2+U^2}\right) \end{bmatrix} \tag{9}
$$

We can find a specific solution if we choose the parameter correctly.

$$
tU = \frac{\pi}{2}\left(4n - 1\right) \qquad t\sqrt{4J^2 + U^2} = \pi m \tag{10}
$$

Where $m$ is an odd integer and $n$ is any integer.

By using these choices eq.(10) and $A = \frac{\sqrt{m^2 - (2n-1/2)^2}}{2m}$ (the solution should be normalized) we get eq. (9)

17

$$i \begin{bmatrix} 1 \\ 0 \end{bmatrix} \tag{11}$$

From eq (11) we get the $\sqrt{SWAP}$ gate .

$$\left( \hat{d_1}^\dagger \hat{u_2}^\dagger - \hat{d_2}^\dagger \hat{u_1}^\dagger \right) \overset{\sqrt{SWAP}}{\to} i \left( \hat{d_1}^\dagger \hat{u_2}^\dagger - \hat{d_2}^\dagger \hat{u_1}^\dagger \right)$$

From these two equations, (10), we can obtain the strength of the interaction $U$ and the time $t$ for which the action will act like a $\sqrt{SWAP}$ gate

$$U = \pm \frac{2J \left( 2n - \frac{1}{2} \right)}{\sqrt{m^2 - \left( 2n - \frac{1}{2} \right)^2}} \qquad t = \frac{\pi \sqrt{m^2 - \left( 2n - \frac{1}{2} \right)^2}}{2J} \tag{12}$$

The last parameter $J$ depend on the distance between the two qubits ,i.e. $d(t)$. One of our goals is to optimize $d(t)$.

### 2.1.4    Ability to Measure the Results

In our system we can detect the population of state $|0\rangle$ ($|-9/2, -9/2\rangle$) in a fluorescence imaging using the cycling transition $|-9/2, -9/2\rangle \to |11/2, -11/2\rangle$. Unfortunately, we can not detect on the cycling transition $|-9/2, -9/2\rangle \to |11/2, -11/2\rangle$ **due to heating**. To overcome this problem, we can measure it with a Raman sideband cooling technique[25] (for more details see section 3.2 ). Recent studies with $^{40}K$ sideband cooling have shown that single atoms release approximately $60 - 80 \, photom/sec$ [13, 14]. In our system assume that can collect $10\%$ we will able to measure one atom fluorescence with EMCCD camera. for shorter detection time we need to tune the probe laser and raise the trap depth.

### 2.1.5    Scalability

In our system the scalability is straight forward. When you already able to initialize and control one qubit, by adding more microtraps you can get a larger number of qubits. The other microtraps are
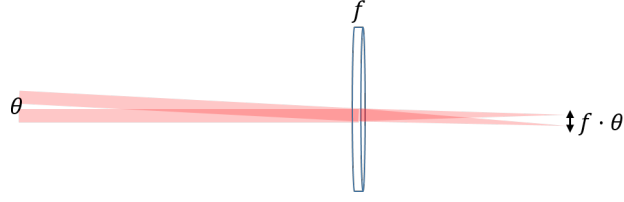
Figure 2: The distance between to traps the reach the lens with an angle $\theta$.

created by other laser beams that reach the the optical objective. These lasers are then focused to different positions at the focal plane:

$$d = f \cdot \theta$$

Where $d$ is the distance between two microtraps, $f$ is the objective focal length and $\theta$ is the angle between the incoming beams (see fig. 2). One way to do it dynamically is by employing two Acousto-Optic-Modulators (AOM), one in x axis and one in y axis [26]. We can position the qubits with $d \gg \lambda$ and then $J \approx 0$. Then the qubits can be brought closer with the optimal $d(t)$. For one qubit gates we can take one qubit to a position where the RF field is optimal and far enough from other qubits (fig. 3).
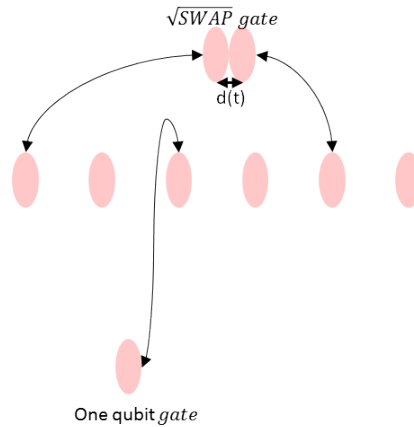


Figure 3: Array of qubits that are formed by AOM. The qubits are moved to the $\sqrt{SWAP}$ region or to the one qubit gate region, according to the quantum code.

The qubit isolation depends on the lifetime in the optical microtrap. we can reduce the laser power

when the atom state is at the ground state and obtain a lifetime of several minutes. Therefore, the decoherence in our system should be very slow. **Furthermore, a ultracold atom system allows for selection of $m$ and $n$ (eq.12) so that the fidelity $\mathcal{F} \to 1$ (the fidelity is the overlap between the chosen target state and the spin state as measured or calculated $\mathcal{F} = \langle \psi_{target} | \hat{\rho} | \psi_{target} \rangle$). This calculation will be done theoretically subsequently.**

## 2.2 Theoretical simulation and calculation

In order to make a numerical calculation of a single atom in a microtrap, we need to solve the time independent Schrodinger equation that is given by

$$H\psi\left(r, \theta, z\right) = E_n \psi\left(r, \theta, z\right) \tag{13}$$

where $E_n$ is the state energy of state $n$ and $H$ is the system Hamiltonian given by

$$H = -\frac{\hbar^2}{2m}\nabla^2 + V\left(r, \theta, z\right)$$

where $V$ is the potential. In 3D the potential of a single microtrap is

$$V\left(r, z\right) = -V_0 \frac{\omega_0^2}{\omega\left(z\right)^2} e^{-2\frac{r^2}{\omega(z)^2}}$$

where $\omega\left(z\right) = \omega_0 \sqrt{1 + \left(\frac{z\lambda}{\pi\omega_0^2}\right)^2}$. The waist of a Gaussian beam is given by $\omega_0 = \frac{\lambda}{\pi \cdot NA}$, where $NA$ is the numerical aperture. The trap parameters are laser beam with $NA = 0.9$ and $\lambda = 1064\,nm$. We calculated the eigenenergies and the eigenstates by solving numerically eq 13. The numerical calculation is 2D taking advantage of the cylindrical symmetry, with 152 divisions in the radial direction and 304 divisions in the axial direction and the accuracy of the results is better than 1%. The result of the calculation is shown in fig. 4. We present calculations in low optical trap $V_0/k_b = 310\,nK$ in order to get one bound symmetric eigenstate. We can see fig 6 that for one bound symmetric eigenstate we need a low depth optical trap.
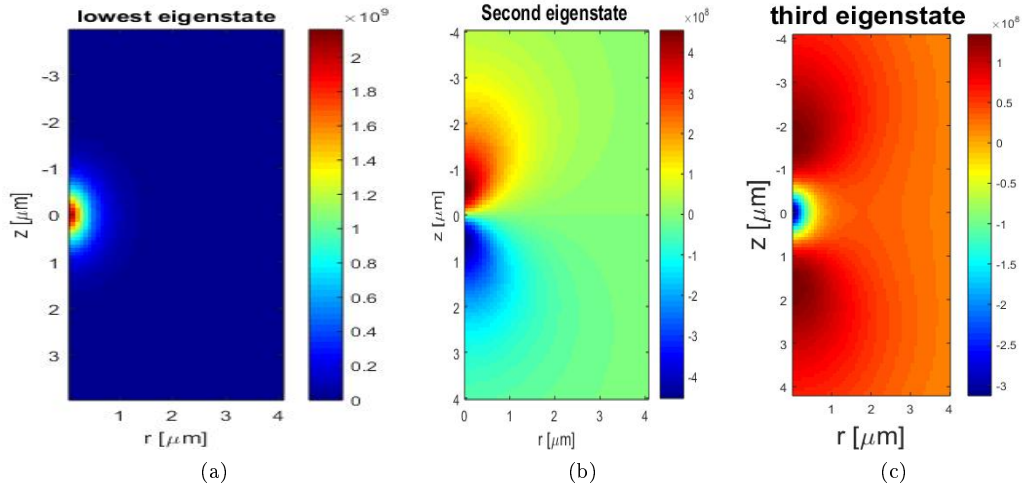
Figure 4: Calculations of bound states in a single Gaussian potential. a) Lowest eigenstate (symmetric) with energy $E/k_b \approx -40\,nK$. b) Second eigenstate with energy $E/k_b \approx -1.5\,nK$ (antisymmetric). c) Third eigenstate with energy $E/k_b \approx -0.316\,nK$ (symmetric). Other states have $E/k_b > 0$ and are therefore not bound.



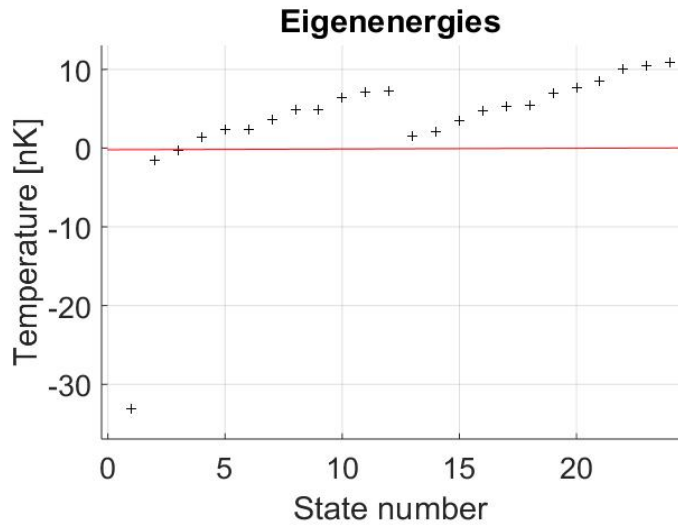Figure 5: Calculations of bound states in a single Gaussian potential. The first 12 is are with $m = 0$ and the next 12 is with $m = 1$, where $m$ is the azimuthal quantum number. There are two bound states ($E < 0$)that are plotted in fig. 4a and fig. 4b.
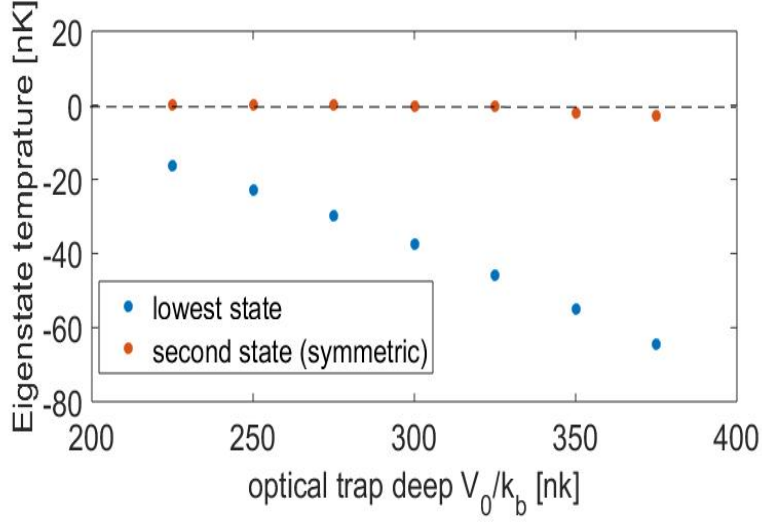
Figure 6: Lowest and second eigenstates energy (in terms of temperature) vs. optical trap depth.

There are many more numerical calculations that have to be done. For example, the gates parameter $U$, $t$, $d\left(t\right)$ (eq 12) for a two qubit gate and one qubit gates parameter that given by eq 2. Another parameter is the transfer qubit trajectory in order to get a fast transfer [27]. All these parameters need to be optimized with demand on the fidelity $\mathcal{F} > 0.99$.

In the next section, I will describe the experimental systems and present our deliberation as to which system would be most worth while for the experiment.

# 3 ultracold atoms

The field of ultracold atoms has seen a rapid development during the last 20 years. Many new experimental techniques have been introduced, and the experimental toolbox has been vastly expanded. Cooling and trapping of atoms is based on the use of forces acting on atoms in laser fields, or on the combination of laser fields and magnetic fields. In this chapter I presents a brief background of cooling and trapping techniques.

## 3.1 Laser cooling technique

### 3.1.1 Doppler cooling

Doppler cooling mechanism was experimentally described in 1978 [28] and it is the basis of our cooling techniques. At a low temperature, kinetic energy sets the temperature by

$$\langle E_k \rangle = \frac{3}{2} k_b T$$

where $k_b$ is a Boltzmann constant. Each time a photon is absorbed by an atom, the atom receives a the recoil momentum $\frac{h\nu}{c}$ in the laser propagation direction. When it emits a photon, it again changes its momentum by the same value but in a random direction. According to this, if the atom travels in the opposite direction to the laser propagation direction the atom will slowdown. However, if the atom moves in the same direction as the laser propagation direction it will accelerate.

In order to slow down and not accelerate the atom, Doppler cooling takes advantage of the Doppler effect, a shift in frequency for an observer moving relative to its source. This means that as the atom moves it experiences a shift in laser beam frequency. When the atom moves towards the laser beam propagation, it will see a frequency shift of $+\delta\nu_D$, and if it moves in the opposite direction to the laser propagation, the shift will be $-\delta\nu_D$. Thus, if the laser frequency is lower than the resonance frequency $\nu_0 - \delta\nu$, the atom which travels in the same direction as the laser will feel ,according to the Doppler effect, $\nu_0 - \delta\nu + \delta\nu_D$. However, the atom which travels in the opposite direction will feel $\nu_0 - \delta\nu - \delta\nu_D$. Accordingly, the atom that travels to the laser will feel the resonance frequency $\sim \nu_0$, but the atom

that travels in the opposite direction of the laser will feel a frequency that is far of resonance $\sim \nu_0 - 2\delta\nu$. Changing the detuning is one way of controlling the magnitude of this force, and drastically affects the number of trapped atoms . Therefore Doppler cooling creates a velocity dependent force. It slows down atoms selectively based on the magnitude of their velocity.

### 3.1.2 Sisyphus Cooling

Sisyphus cooling (polarization gradient cooling) is a laser cooling technique which was observed experimentally and later first given a full explanation by Claude Cohen-Tannoudji [29]. Sisyphus cooling is achieved by two orthogonal polarization laser beams. The two lasers create a polarization lattice. When the atoms move to the maximum of the potential (and the resonance frequency is closer to the laser frequency) they lose kinetic energy and move slower. As they reach the maximum they are optically pumped to the minimum as show in fig. 7a. In $^{40}K$ this technique does not work due to narrow and inverted hyperfine structure of the $P_{3/2}$ state [30].

### 3.1.3 Gray Molasses Cooling

Gray Molasses is a cooling technique very similar to Sisyphus cooling. The difference between them is that in Gray Molasses the electromagnetic field splits the energy levels to a dark state and bright states. If the laser beam is blue detuned, the bright level is light-shifted and the dark state does not change (since it is not coupled to the light field). Similar to Sisyphus cooling, the atoms "climb" to the maximum of the potential well and then pumped to the dark level (see figure 7b). In a general principle, a better cooling scheme is one that the coldest atoms are pump to a dark state and they are not heated by spontaneous scattering events. Recent studies [31, 32] showed that for $^{40}K$ Gray mollases on the $D_1$ line can reach a temperature of $T \sim 15\,\mu K$ .
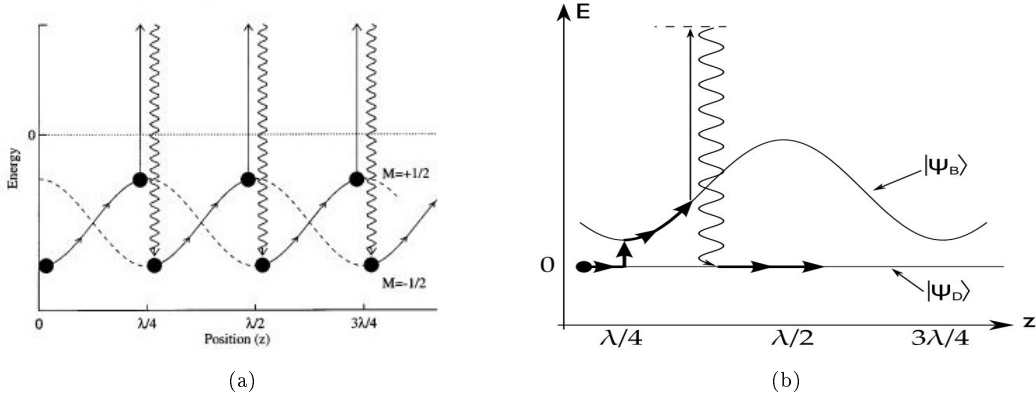
Figure 7: a) Sisyphus cooling scheme. Adopted from ref. [33] b)Gray molasses cooling scheme. With positive detuning the ground state splits to two states $|\psi_D\rangle$ and $|\psi_B\rangle$. These two states act like the states in Sisyphus cooling. Adopted from ref.[32].

### 3.1.4   Magneto optical trap

A Magneto Optical Trap (MOT) consists of laser beams propagation and retro-reflecting along three orthogonal directions and coils with anti-Helmholtz configuration. The laser beams with red-detuning from an energy transition in the potassium spectrum are sent to the atoms. The main mechanism is a Doppler (3.1.1) effect [34]. The red-detuned (light with a frequency smaller than the resonance frequency) light is Doppler shifted in the rest frame **of a moving atom to a frequency at which atom is closer to the resonance frequency are interact with the laser beam**. This shift causes the atoms to interact with the laser as if they are moving opposite the lasers propagation direction. We cool the atoms by lowering their velocities. However, in this process, there is a limit [34] to the temperature

$$T_D = \frac{\hbar\Gamma}{2k_B}$$

where $k_B$ is the Boltzmann's constant, $\hbar$ is the reduced Plank's constant and $\Gamma$ is the natural line-width. In $^{40}K$ the Doppler limit is $T_D \sim 150\mu k$.
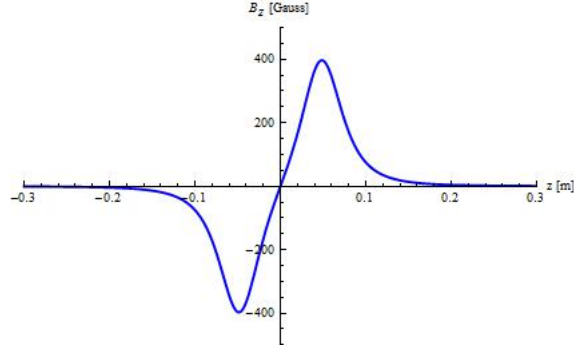
Figure 8: The magnetic field created by anti-Helmholz configuration

### 3.1.5 Magnetic field for MOT

Doppler cooling lowers the temperature of atoms, but does not differentiate between an atom far from the middle of the trap and one at the center. A magnetic field takes advance of the Zeeman effect to localize the atoms and to increase the density.Atoms can have different angular momentum $m_z = -f, -f + 1, .., f$ where $f$ is the total atomic spin. In the presence of a magnetic field, the energy levels are split into sub-levels. The energy change is given by:

$$\Delta U = -\vec{\mu} \cdot \vec{B}$$

where $\vec{\mu}$ is the magnetic dipole moment of the state and $\vec{B}$ is the magnetic field. Therefore, the energy difference is proportional to the magnetic field and depends on its direction.

Coils with anti-Helmholtz configuration produce a magnetic field that switch its sign at the origin (see figure 8 ). This give two regions: positive and negative. At the origin the magnetic field is zero. Therefore, the energy shift is $\Delta U \approx 0$ . In the positive magnetic field, the $m_z < 0$ and will have increased energy and in the negative magnetic field, the $m_z > 0$ and will have decreased energy. ($\Delta U$ go opposite to the magnetic field). Therefore, as shown in figure 9 , a photon with the correct polarization , will be confined by the atoms by giving a spatially dependent forces with zero force in the center. In fig. 10 I summarized the laser directions and polarization in 3D due to magnetic field from quadratic coils.
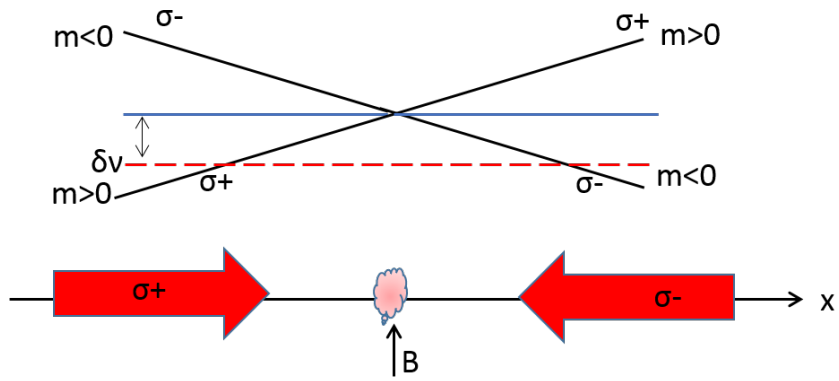
26

Figure 9: Description of Zeeman split and polarization of laser beams with detuning $\delta\nu$ in one dimension. The blue line is the energy level at zero magnetic field. On the left the magnetic field is negative therefore the atom interacts with $\sigma^+$ laser polarity .In the right side the magnetic field is positive so the atom interacts with $\sigma^-$laser polarity.
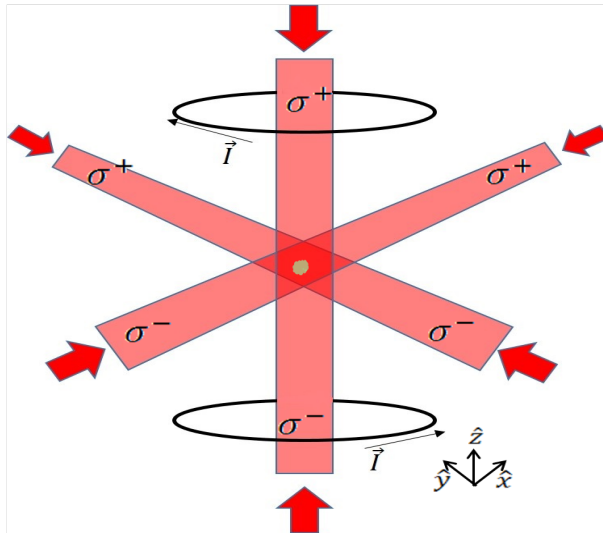


Figure 10: MOT configuration

## 3.2 Raman Sideband cooling

In order to describe Raman sideband cooling, we need to explain what is a Raman transition [35]. Raman transition is a two photon transition consisting of absorption and stimulated emission. **As show in fig 11a an atom moving with velocity $v$, that absorbs a photon of frequency $\omega_1$, exciting it into a virtual state $\delta$ detuned from the upper level $|c\rangle$. Immediately, another photon with frequency $\omega_2$, traveling in the opposite direction causes stimulated emission of the photon into state $|b\rangle$.** This allows for the precise selection of atoms with velocities that satisfy the equation

$$\frac{v}{c} = \frac{\omega_0 - (\omega_1 - \omega_2)}{\omega_1 + \omega_2}$$

where $c$ is the light speed and $\hbar\omega_0$ is the transition energy between $|a\rangle$ and $|b\rangle$.

We can use the Raman pulse to transfer an atom with velocity $v$ from $|a\rangle \rightarrow |b\rangle$ and with another laser we can excite the atom from $|b\rangle \rightarrow |c\rangle$. At state $|c\rangle$ the width of the velocity distribution is $\sigma_c(v) \ll \sigma_a(v)$. Therefore when the atom decays back to $|a\rangle$ with velocity around $v - v_r$, at the end of the cycle we have more atoms with lower velocity. In 1995 Wineland *at el.*[25], proposed cooling an atom to the ground state in a 3D optical trap scheme that was based on Raman transition. Only recently and with more sophistication, it was carried out with $^{40}K$ [13] in an optical lattice. By cooling with Raman sideband technique we gain two benefits. First, we can detect the number of atoms at each site due to their fluorescence, and second, we can lower the atom to the ground state.

## 3.3 Magnetic trap - Quic configuration

One cooling technique in ultracold atoms experiments is RF evaporation [36]. In this technique the atoms are loaded to magnetic trap with $m_z > 0$ and by using RF field the atoms are transferred to state with $m_z < 0$ which is not magnetically confined and therefore they leave the trap. In this technique , if the minimum of a magnetic field is zero the atoms that are closer to the minimum (with low temperature) can flip their spin and be ejected. A QUIC configuration trap [37] is formed by two quadrupole coils and one Ioffe coil. The MOT uses the same coils as the quadrupole trap, so the transfer of atoms from the MOT into the magnetic trap is straightforward. Atoms are loaded into a
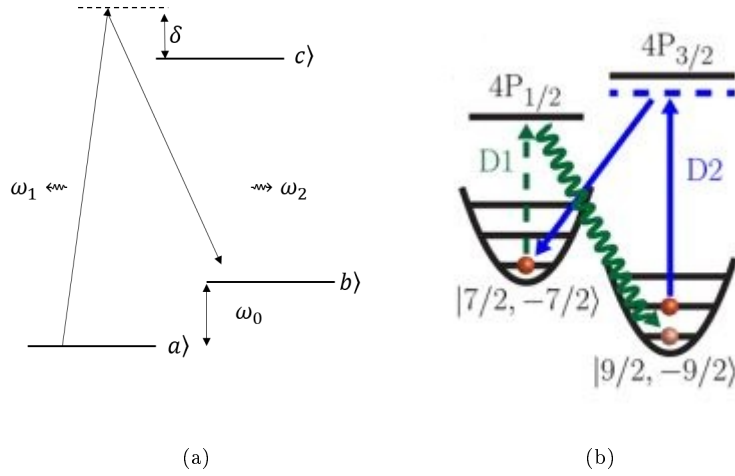
28

Figure 11: a) Raman transition between two atomic levels $|a\rangle$ and $|b\rangle$ b) Raman sideband cooling scheme in $^{40}K$ taken from [13].

quadrupole trap and subsequently transferred to an Ioffe type trap. As shown in fig (12) the magnetic field goes from quadrupole with $\min(B) = 0$ to quadrupole with $min(B) = 1$ G and the minimum is shifted around 17 mm towards the Ioffe coil. The ratio between $\frac{I_I}{I_Q}$ depends on the exact sizes of the coils and distance between the quadrupole coils and the Ioffe coil.
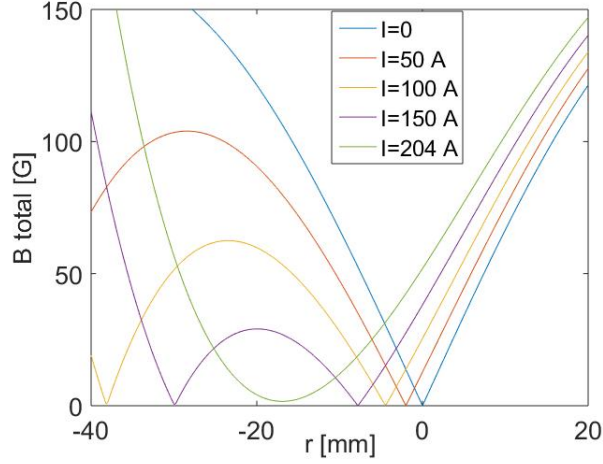
Figure 12: Magnetic field calculations in $y$ direction starts with quadrupole with $I_0 = 210\,A$ and the addition of a Ioffe coil with different current. The minimum is adiabaticlly moved $\sim 17\,mm$ towards the Ioffe coil.

## 3.4 Optical trap

Optical dipole force comes from the potential that an atom feels when the oscillating electric dipole moment of the atom, induced by the oscillating electric field of the laser light, interacts with the field. Two important quantities for optical dipole traps are the depth of the potential $U_{dip}(r)$ and the scattering rate $\Gamma_{sc}(r)$. In terms of decay rate they can be expressed as [38]

$$U_{dip}(r) = \frac{3\pi c^2 \Gamma}{2\hbar \omega_0^3 \delta} I(r)$$

$$\Gamma_{sc}(r) = \frac{3\pi c^2 \Gamma^2}{2\hbar \omega_0^3 \delta^2} I(r)$$

where $I(r)$ is the laser beam intensity and $\delta = \omega - \omega_0$ is the frequency detuning of the laser from the frequency of the optical transition $\omega_0$. The dipole trap can be attractive for red detuning $(\delta < 0)$ or repulsive for blue detuning $(\delta > 0)$.

| $\lambda$ | $P\ [mW]$ | $lifetime\ [msec]$ |
|---|---|---|
| 1064 | 75 | 220 |
| 820 | 20 | 23 |

Table 2: Comparison of the life time and the laser source power in two commercial laser wavelengths. We required a $1\ mK$ trap which is high enough for atoms at temperature following $D_1$ cooling ($T_{D_1} \sim 30\mu K$).

The simple example is for $TEM_{00}$ Gaussian mode with far of resonance frequency. Beam intensity is given by

$$I\left(r,z\right) = \frac{2P}{\pi\omega^2\left(z\right)}e^{\frac{-2r}{\omega^2(z)}}$$

Where $\omega\left(z\right) = \omega_0\sqrt{1 + \left(\frac{z}{z_R}\right)^2}$. The peak intensity is given by $I_0 = 2P/\pi\omega_0^2$. The trap depth is defined as $U_0 = |U\left(0,0\right)|$ and linearly proportional to the beam intensity. Expanding around the position of maximum intensity leads to a harmonic potential

$$U_{dip}(r,z) = -U_0\left[1 - 2\left(r/\omega_0\right)^2 - \left(z/z_R\right)^2\right] \tag{14}$$

# 4 The experimental machines

In our lab we built an ultracold atoms system with $^{40}K$. In this chapter I will describe the systems and concentrate on the parts I constructed.

## 4.1 The experimental systems

We considered two methods (see sketches in fig 13) of creating a single atom trapped in a optical trap Each of these methods has advantages and disadvantages, as we describe below, and at this point. We have not yet decided which one to use. We plan to advance in both before make the final decision. Considerations are the preparation time of a single atom trap and the temperature of the atom. The first system is a machine producing as an initial resource a quantum degenerate Fermi gas with $T/T_f \ll 1$. The second method is characterized by loading from only a relatively ultracold cloud after 3D MOT or $D_1$ cooling, removing all atoms other than one, and then cooling inside the trap.

1. **Degenerate fermi gas.** The first system (see fig. 13a) is composed of 3 cells under ultrahigh vacuum $\sim 10^{-11}$ $torr$ . In the first cell ("source") we release $^{40}K$ atoms from home made dispensers. The atoms are captured by a 2D MOT. On the third axis there is a mirror with a hole (nozzle) inside the chamber. The atoms are cooling in two axes and pushed to the second cell by another laser (with different detuning ) in the third axis (reflected with hole in the middle by a nozzle). In the second cell they are captured and trapped by a 3D MOT. At this point, the cloud temperature is around $\sim 220\mu K$ set by Doppler limit. By using a Gray Molasses cooling on the $D_1$ atomic transition, the atomic cloud temperature is reduced to $\sim 15\mu K$. Next, we optically pump the atoms into the states$|9/2, 9/2\rangle$ and $|9/2, 7/2\rangle$ and load the atoms to a magnetic trap with a QUIC configuration [37]. In this configuration, we get a magnetic trap without $B = 0$. This is important for a $RF$ evaporation. Following the evaporation, the temperature is $T/T_f \approx 1 - 3$. Next we load the atoms to a far of resonance optical trap and move the optical trap adiabaticlly (with air bearing stage ) to the science chamber. Then, we first make sure that the cloud is spin polarized, and then load it to a microtrap and reduce the

trap depth until there is only a single bound state [17].

The advantages of this approach is that the process of cooling happens prior to loading, and there is a large spatial separation between the source and the final trap (which ensure a long lifetime of the trapped atom) and a greater density of atoms. The disadvantage is that the process is rather complicated and takes around 80 seconds.

2. **Fast approach.** In the second system (see fig. 13b)we have one cell under high vacuum $\sim 10^{-11}$ $torr$ . The $^{40}K$ atoms will be released from a home made dispenser by heating and trapped with a 3D MOT. Then, by using a Gray Molasses cooling on the $D_1$atomic transition we will get a cloud with temperature of over hundreds of micro-kelvin. Next, we can load directly to a micro-trap made of a far-off-resonance light. Then, using light assisted collisions,only a single atom will remain trapped. This single atom is "hot" in the sense that its spread over vibration states is large. In order to measure the atom and to cool it to ground state, we plan to use Raman side-band cooling [25, 13, 14].

The advantages of this approach is simplicity of the apparatus and the short duration of the experiment which allows for fast data accumulation rate. The disadvantage is a shorter lifetime due to the residual ambient gas. There is also a possibility to construct a system made of two chambers, where one chamber is used with 2D MOT to generate a source.

We are currently building two experimental systems: the first one is a degenerate fermi gas machine where we will be able to proceed with the first approach (this system is planned to be used also for other experiments), and a second smaller system in which we are going to explore the second approach. The first one, we started to construct two years ago, and in the meantime we completed the 2D and 3D MOT, $D_1$ cooling, optical pumping, magnetic trapping in QUIC trap, RF evaporation, loading in to an optical trap, transporting the atoms to the science chamber. The second system we started to build eight months ago (the vacuum chamber was actually evacuated two and a half years ago), we have just one cell and we've completed the 3D MOT and now working on loading atoms to the optical microtrap and detecting them.
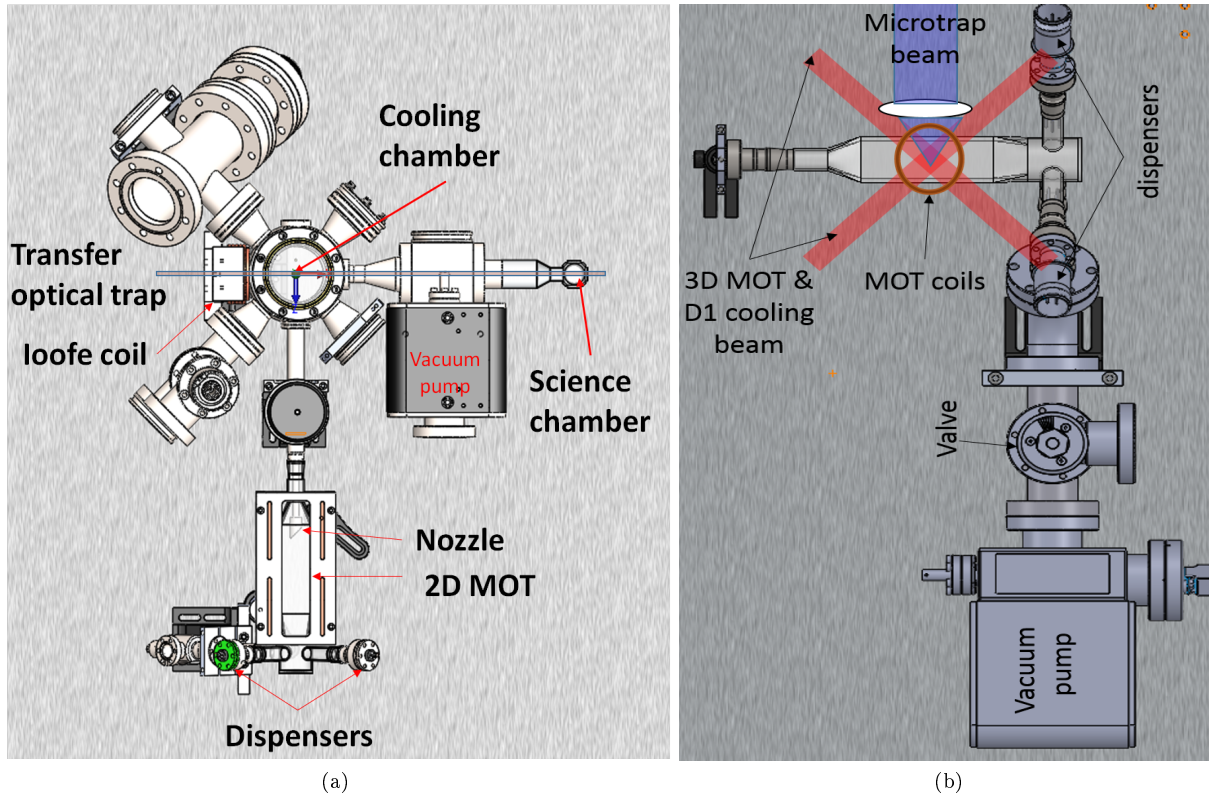
Figure 13: a) Degenerate fermi gas system description. Atoms are released from the dispensers and are trapped by a 2D MOT in the first cell ("2D"). In the second cell ("cooling"), atoms are trapped by a 3D MOT and cooled with $D_1$ cooling and RF evaporation. Then, they are loaded to an optical trap that transfers the atoms to the third cell ("science"). b) Fast approach system (with one cell) description. This chamber is like the 2D MOT chamber in the first system. Atoms are released from the dispensers and trapped by 3D MOT. Then the atoms are loaded into an optical microtrap.

## 4.2 MOT

In both system the first stage is MOT. In the first method we started with a 2D MOT and continued to a 3D MOT and in the fast approach method we start with a 3D MOT. In the first system we first used a 2D MOT as described in [39]. For the 3D MOT we needed, as explained before, two lasers (cooling and repump) and two coils with anti-Helmholtz configuration. In this configuration we can not make RF evaporation as there is a zero magnetic field at the bottom. Therefore, we added a Ioffe coil in a QUIC configuration [37].

### 4.2.1 Coils setup

I made three coils from a $4.2x4.2\ mm$ square copper tube, which is hollow in order to cool the coil at a high current by letting water flowing through it. To wrap this coil, we have designed a part made of Teflon that connects to a rotating spindle (14b). Teflon is important for two reasons, one so that the glue will not stick to the holder, and the other to avoid harming the coating of the coil. After each round we smeared a layer of glue *(Araldite 2011)* and let it dry for 24 hours.

Taking into account the dimensions of our system we need two coils (both for the 3d MOT and for the magnetic trap) with *7X5* winding with $r = 20\ mm$. Another coil with *6X4* and an inner most radius of $r = 30\ mm$(14a). The coil current is controlled with a PID loop which measures the current by Hall probe.
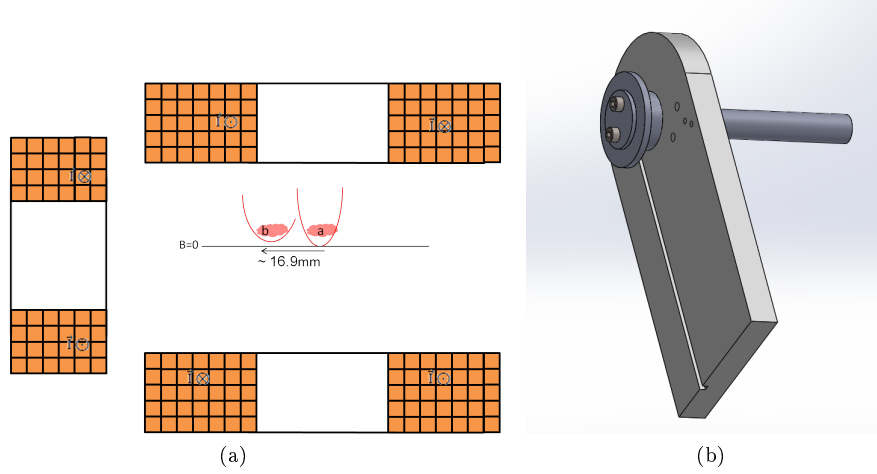
Figure 14: a) Quic configuration. Atoms are loaded at point a, by two coils with anti-Helmholtz configuration with $U_{min} = 0$. when the Ioffe current rises, the atoms are moved to the new minimum, at point b ($d = \sim 16.9\ mm$), with $B_{min} \approx 1\ G$. b) Picture of the part which twisted the coils.

### 4.2.2 Lasers setup

For MOT, we need two lasers: one for cooling and the other as a repump, to return the atoms to the cooling transition if they end up in the other hyperfine state $m_f = 7/2$ . In our setup, as show in fig (15), we used one laser as a reference laser (DBR laser *PH770DBR080T8* from *Photodigm* and a current and temperature controller of *LDC 501* from *Stanford Research System*). The reference laser is locked on the $|F = 2\rangle \rightarrow |F' = 3\rangle$ on the $D_2$ transition in $^{39}K$. The reference laser is locked to room temperature on the vapor cell with $^{39}K$ atoms, hence we need to use Saturated Absorption Spectroscopy (4) . The two other lasers are locked with Offset locking [40] to the reference laser. I chose that configuration as I needed a wide tunability range for the lasers (we can not get that by using AOMs). Theoretically, the shift between the reference laser to the cooling laser , as describe in fig (16), is

$$f_{\text{cooling}} = f_{\text{reference}} + 804.85\ MHz$$

I placed an AOM as a switch before the fiber with $-100MHz$ shift and I determined a red detune of $3\Gamma \approx 18\,MHz$. Therefore
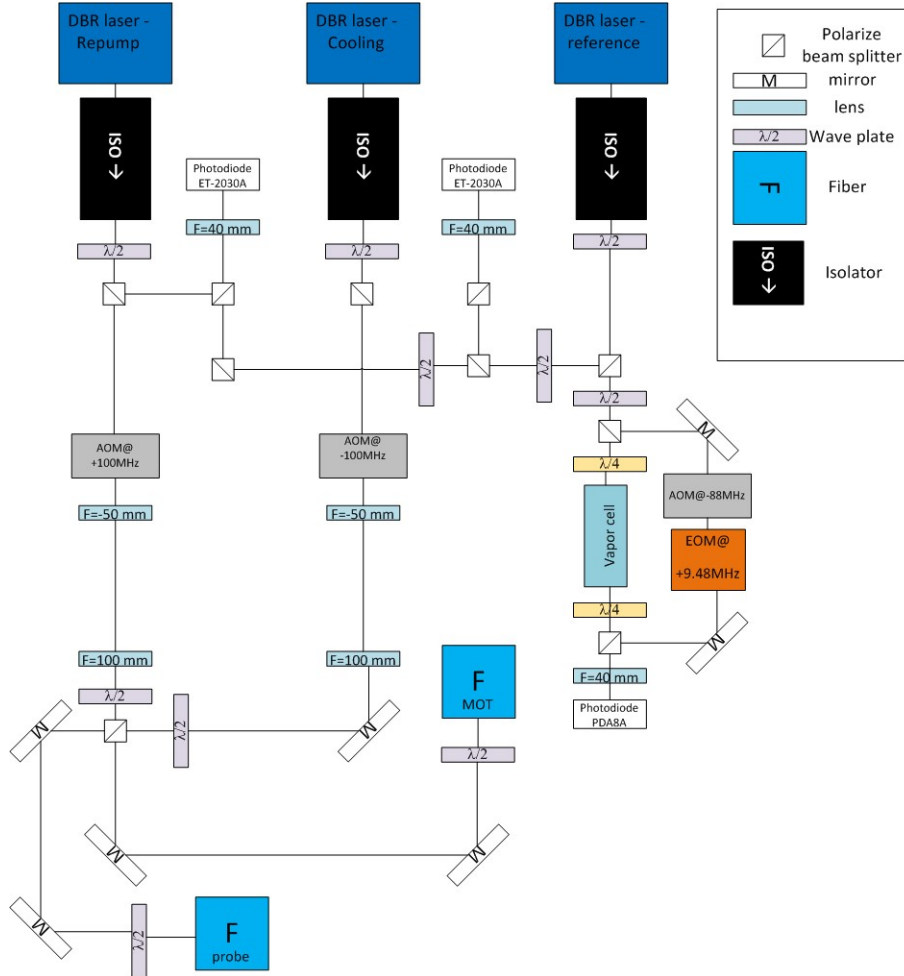
$$\Delta f_{coolng} = 922\,MHz$$

In addition, the theoretical shift between the reference laser to the cooling laser is

$$f_{repump} = f_{reference} - 431\,MHz$$

I placed a AOM as a switch before the fiber with $+110\,MHz$ shift, and I determined a red detune of $3\Gamma \approx 18\,MHz$. Therefore

$$\Delta f_{coolng} = 522\,MHz$$

Figure 15: Laser setup. Cooling and repump are locked by offset locking to the reference laser. The reference laser locked on $|F = 2\rangle \rightarrow |F' = 3\rangle$ in the $D_2$ transition of $^{39}K$ with SAS system. Most of the power of the lasers (cooling and repump) goes through a AOM which is used as a switch. After a 1:2 telescope they are split and the most injected to one fiber that leads to the MOT. The other power injected to another fiber that lead to the probe.
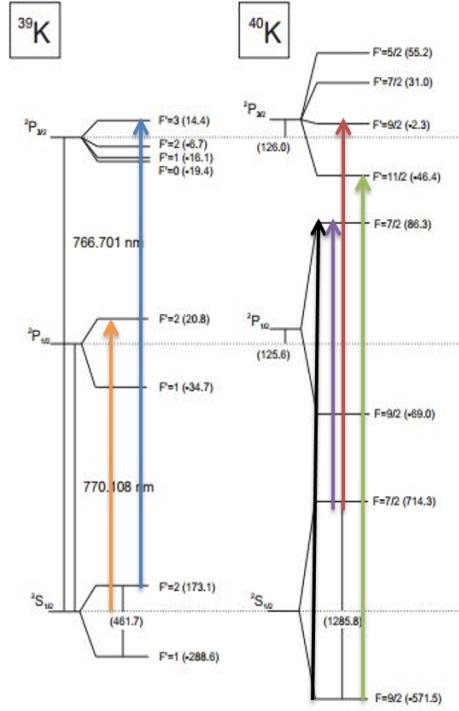
Figure 16: Optical transitions of the $D_1$ and $D_2$-lines of $^{39}K \& ^{40}K$. Blue Arrow is the transition which we lock to using the Saturated absorption spectroscopy for the MOT. Orange arrow is a transition used for the $D_1$ cooling. Green Arrow is the cooling transition and the red arrow is the repump transition for the MOT. Black Arrow is the cooling transition and the purple arrow is the repump transition for the D1 cooling. The numbers are in $MHz$. Adopted from [41]

### 4.2.3 Saturated Absorption Spectroscopy (SAS)

In laser cooling, we must lock the laser to the frequency of an atomic transition. The atoms move with a random velocity distribution, so the laser comes into resonance with different velocity groups of atoms. Therefore, the laser interacts with atoms in different velocity groups of atoms. Their velocities, according to Maxwell-Boltzmann distribution, are

$$\frac{dn}{dv} = n_0 \sqrt{\frac{m}{2\pi k_b T}} exp\left(\frac{-mv^2}{2k_b T}\right)$$

If the laser beam is at frequency $f_0$ in the reference frame of the lab, in the atoms frame the frequency is shifted due to the Doppler effect:

$$f = \left(1 \pm \frac{v}{c}\right) f_0$$

This means that each velocity group has a different resonance frequency in their respective frame of reference. Therefore, the frequency assumes a shape of Gaussian

$$I(f) = I_0 exp\left[-\frac{mc^2 (f_0 - f)^2}{2k_b T f^2}\right] \tag{15}$$

with a width of $\sigma = f_0 \sqrt{\frac{k_b T}{mc^2}}$. In $^{39}K$ on temperature $T \approx 340\,k$ the width $\sigma = 346\,MHz$ Doppler broadening makes it impossible to determine the precise transition frequency to within the natural linewidth ($\Gamma \sim 6\,MHz$). To overcome this difficulty, we need to use an SAS system which is a probe pump setup.

Two counter-propagating , probe and pump, laser beams derived from a single laser beam are sent through an atomic vapor cell (in our case a vapor with $^{39}K$) at room temperature with same frequency $f_0$. A photodiode is placed after the vapor cell and measured the probe beam. If the probe beam frequency is not at the resonance frequency ,$f_{\text{probe}} \neq f_0$, then it will interact with atoms whose have velocity $v$ that satisfy the the Doppler shift $f_{probe} = f_0 (1 + v/c)$. In addition, the pump beam will interact with atoms whose have velocity $-V$. In this case, the signal on the photodiode will be a deep (eq. 15) with width of $\sigma$,But, when the beam is on resonance $f_{probe} = f_0$, the atoms with zero velocity, there is a sharp decrease in absorption (seen as a sharp increase in the signal from the detector), since many of these atoms have been pumped out of the ground state, and will not be able to absorb any photons from the resonant probe beam. In figure 17a I show the signal from SAS system with with $^{39}K$ at room temperate for the $D_2$ laser and in figure 17b I show another SAS system result for the $D_1$ transition. The system description in in fig 15 for $D_2$ and in fig 24 for $D_1$.
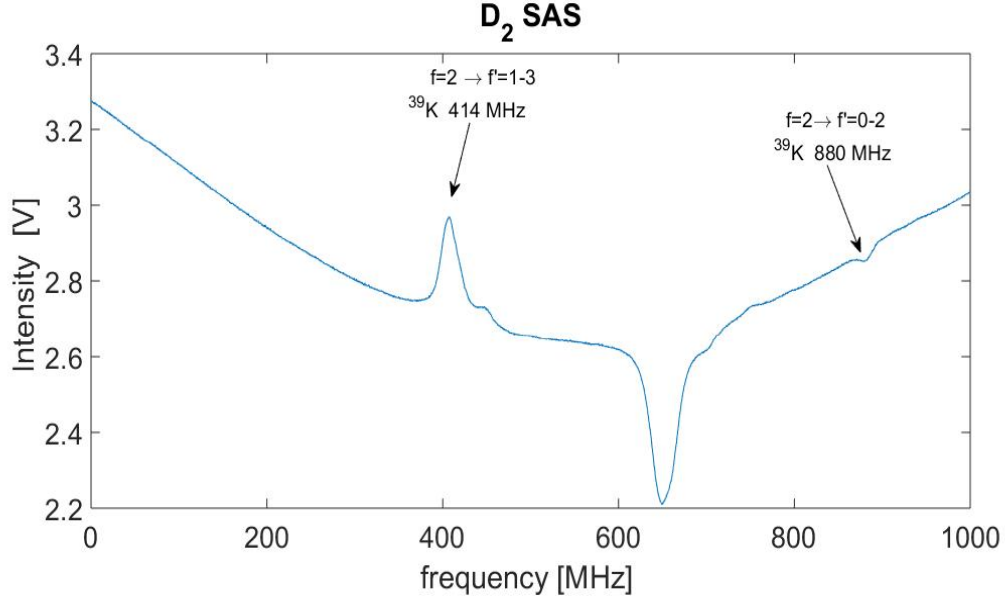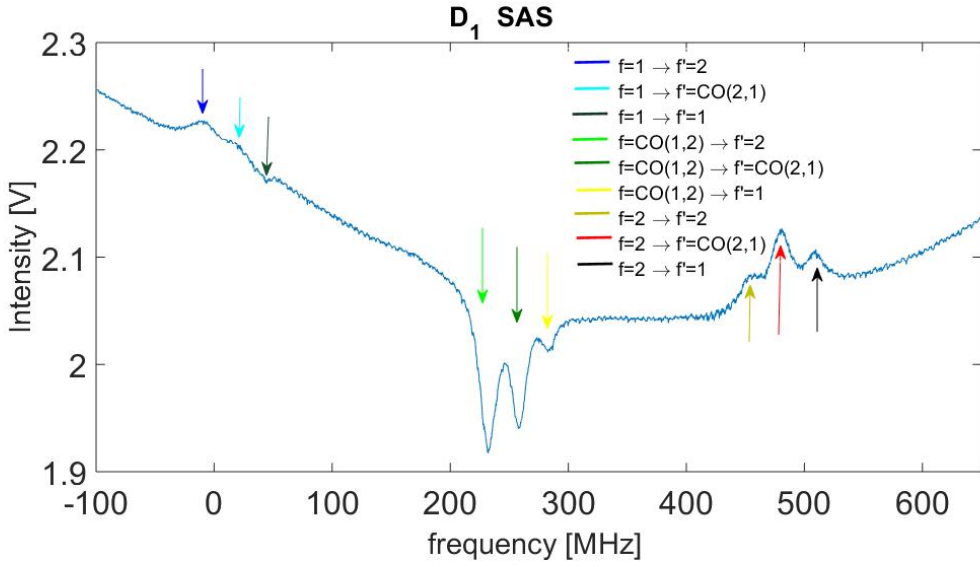
Figure 17: Saturated Absorption Spectroscopy in our system. Figure a) is for the $D_2$ transition (fig.16) where zero frequency is for the repump transition in $^{40}K$ and in figure b) is for the $D_1$ transition (fig.16) where zero frequency is the transition between $F = 1 \rightarrow F' = CO\,(1,2)$ in $^{39}K$.

### 4.2.4   Offset locking

Offset locking is a technique to lock a laser to the reference laser and give the ability of frequency tuning from tens of MHz to several GHz. This technique is based on the frequency depended phase shift, experienced by the beat note of two laser frequencies as shown in [40].The circuit and the locking signal are show in fig 18.
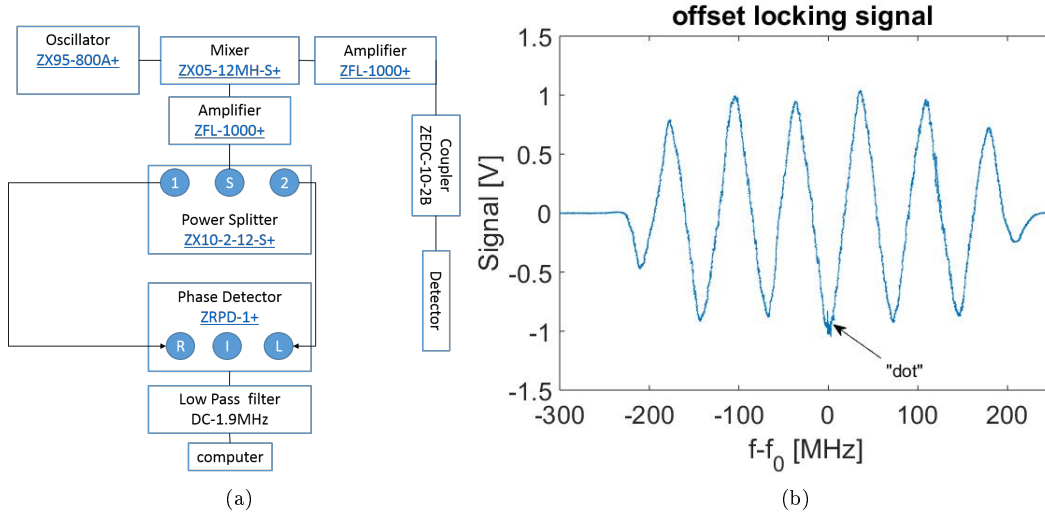


Figure 18: a) Offset Locking circuit. The signal is go throw a coupler (ZEDC-10-2B) in order to take a reference of the signal (and measure the laser width) and amplify (zfl-1000+). Then it mixed (zx-12MH-S+)with a voltage control oscillator (zx95-800A+). It then splits to two line (ZX10-2-12-S+), one short and another long (0.1m & 3.4m). After that, the two lines are recombined on a phase detector (ZRPD-1+). We use a low pass filter of 1.9KHz at the end. b) offset signal. The "dot" possition is controled by the VCO

### 4.2.5   Measurements of the number of atoms

In order to calculate the number of atoms we measure their florescence with a photodiode. We can calculate the number of atoms by:

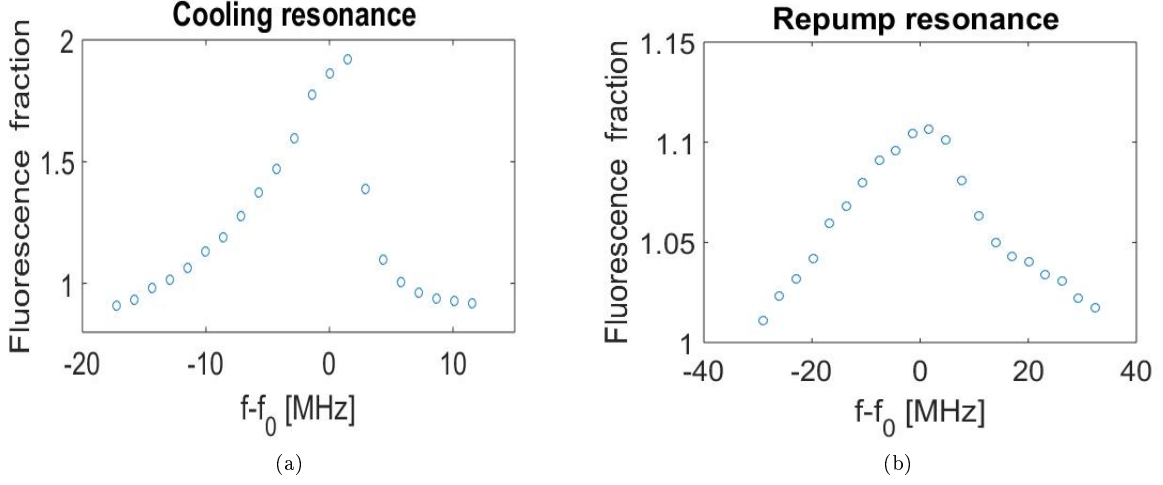$$N = \frac{V\tau}{g_1 g_2 S \cdot E_{photon}\rho_6}$$

Figure 19: Calibration of the resonance frequencies. a) Cooling Laser Fluorescence Fraction. b) Repump Laser Fluorescence Fraction

where $V$ is the measured output voltage, $\tau$ is the excited state life time of the atom, $g_1$ is the current to voltage photodiode gain , $g_2$ is the photodiode efficiency, $S$ is the solid angle fraction $\left(S = \arctan\left(\frac{d}{f}\right)\right)$, $E_{photon}$ is the photon energy and $\rho_6$ is the excited state fraction that is calculated in [42] for a six level model.

In order to calibrate the laser detuning, we first find the resonance. We load the MOT for 15 second with cooling laser frequency at $f_0$ optimized for MOT operation and then change in 10 millisecond the cooling laser frequency to $f_1$ and then measure the fluorescence fraction $\frac{V(f_1)}{V(f_0)}$ . By performing this sequence, we make sure our signal does not depend on the number of atoms and $f_0$, but only on $f_1$ . The result is shown in fig(19a).We repeat this measurement also for the repump laser (fig. 19b). Now, we optimized the lasers detuning (cooling and repump) in order to get a high number of atoms (see
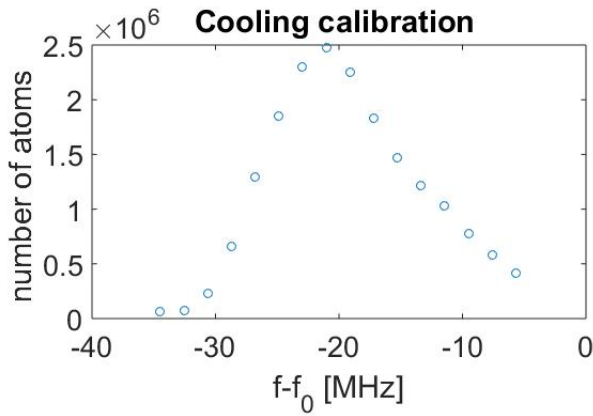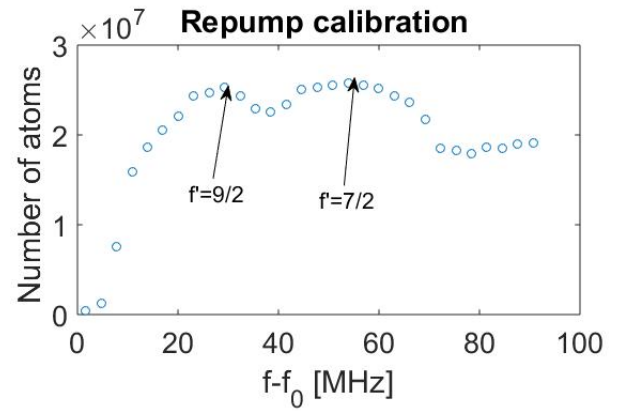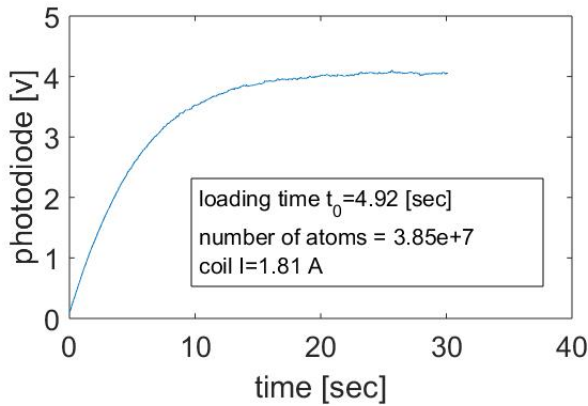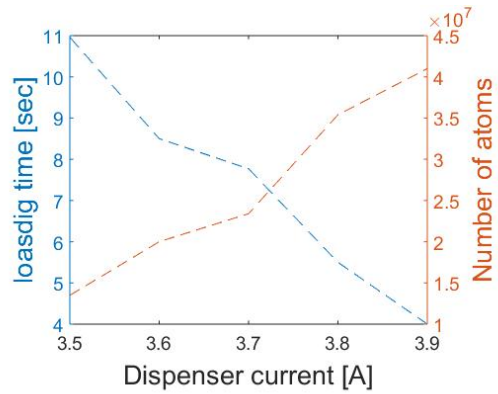
Figure 20: Number of atoms vs laser frequency. In order to know what are good conditions for the MOT, we scan the laser frequency and calculate the number of atoms . (a) Cooling Laser. (b) Repump Laser



Figure 21: a) Example of loading time measurement. b) Number of atoms and loading time vs. dispenser current. High currents release more potassium-40 and therefore, increases atoms density in the cell . As a result, the loading time decreases and the number of atoms increases. However, a high current shortens the life of the dispenser.

| | $\delta t_1$ | $\delta t_2$ | $\delta t_3$ | $\delta t_4$ |
|---|---|---|---|---|
| MOT at $t_0$ | ● | ● | ● | ● |
| release | ● | ● | ● | ● |
| recapture | ◉ | ◉ | ◉ | ◉ |

Figure 22: Release & Recapture Experiment. In a short time most of the atoms do not escape from the area of the MOT beams so they are trapped again. However, as time exceeds, the number of atoms that remain in the MOT beams decreases, depending on their velocity or, in other words, their temperature.

fig 20a and fig 20b).

The last parameter that is tunable is the dispenser current. The dispenser current can shorten the loading time (fig. 21) and increase the atoms number.

### 4.2.6 Temperature Measurement with Release & Recapture Technique

In order to measure the MOT temperature we use Release and Recapture (R & R) method [43] described in fig(22). Assuming that the atoms in the MOT have a Maxwell Boltzmann distribution

$$f\left(v\right) = 4\pi v^2 \left(\frac{m}{2\pi k_B T}\right)^{3/2} e^{-\frac{mv^2}{2k_B T}}$$

At some point we immediately shut off the trap and let the atoms expands ballistically for duration $\delta t$ and then open the lasers again and recapture part of the atoms. The position of each atom after this expansion is given by

$$f\left(r,t\right) = \frac{4r^2}{\sqrt{\pi}\alpha^3 t^2} e^{-\frac{r^2}{\alpha^2 t^2}}$$

Where $\alpha = \left(\frac{m}{2k_B T}\right)^{-3/2}$. Now we can use $v = r/t$ and get

$$f\left(v\right) = \frac{4v^2}{\sqrt{\pi}\alpha^3} e^{-\frac{v^2}{\alpha^2}}$$

45

**R&R measurement**

(a)

(b)

| Model | erf1 (User) |
| --- | --- |
| Equation | erf(A/x)-(2/sqrt(pi))*(A/x)*exp(-(A/x)^2)-b0 |
| Plot | fraction |
| A | 0.01247 ± 2.5852E-4 |
| b0 | 0.01552 ± 0.00887 |
| Reduced Chi-Sq | 9.63839E-4 |
| R-Square(COD) | 0.99259 |
| Adj. R-Square | 0.99229 |

T=247 uK
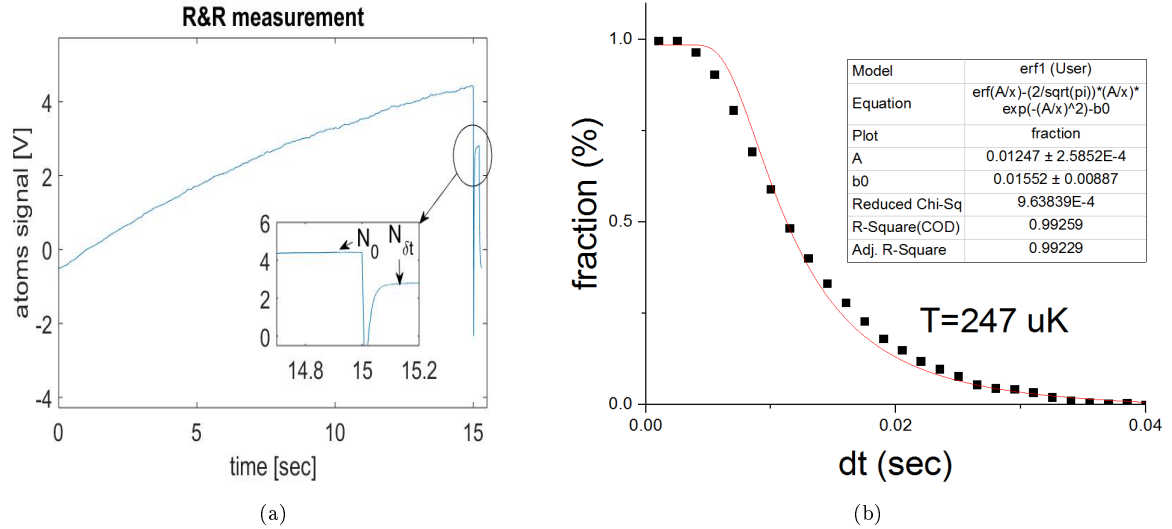
Figure 23: Release & Recapture Measurement. a) Example of sequence. We loaded the MOT and closed the lasers for $\delta t$ and calculated the fraction of $\frac{N_{\delta t}}{N_0}$. b) Fraction vs. $\delta t$. From the fit, I calculated the temperature and found $T \approx 247 \mu k$.

Assuming that the MOT radius starts with $r_0$ and captures with the radius beam ($r_f = \omega_0$), we can calculate the number of atoms that we trap

$$N\left(t\right) = \int_{r_0}^{r_f} N_0 f\left(v\right) dv = N_0 \frac{4}{\sqrt{\pi}\alpha^3 t^3} \int_0^{\omega_0} r^2 e^{-\frac{r^2}{\alpha^2 t^2}}\, dr$$

$$\Rightarrow \frac{N\left(t\right)}{N_0} = erf\left(\frac{\omega_0}{\alpha \cdot \delta t}\right) - \frac{2\omega_0 e^{-\frac{\omega_0^2}{\alpha^2 \delta t^2}}}{\alpha \cdot \delta t \sqrt{\pi}}$$

I measured the fraction of the number of atoms in the MOT after $\delta t$ without lasers divided by the number of atoms before closing the trap (the result are show in fig (23)). We measured the MOT laser

waist $\omega_0 = 4.4\,mm$ and got $\alpha = 0.01247 \pm 0.00258$. Therefore the temperature is $T = 274 \pm 13 \mu k$.

## 4.3 $D_1$ cooling

As explained in 3.1.3, $D_1$ cooling can lower the temperature to $T \approx 15 \mu K$ in $^{40}K$ without atom loss. Below I introduce our system and experimental results.

### 4.3.1 Lasers setup

We used a DBR laser (*photodigm PH770DBR080T8*) at $\lambda = 770.1\,nm$ and a current and temperature controller ( *Stanford Research System LDC501*). We took a $\sim 10mW$ towards an SAS system (4) . We locked the laser with the derivative signal by a PID loop on the current of the laser.

The $D_1$ cooling transition is $|F = 9/2\rangle \rightarrow |F' = 7/2\rangle$. However, we used a $^{39}K$ for locking the laser and the most obvious line in locking signal is the crossover line $|F = co\,(1,2)\rangle \rightarrow |F' = 2\rangle$. As we can see ??, to obtain the transition $|F = 1\rangle \rightarrow |F' = 2\rangle$ we need to add $230.85\,MHz$ .Now we need to move to the energy level of $^{40}K$. Therefore the cooling resonance is:

$$f_{cooling} = f_{lock} + 704.85\,MHz$$

We mange this with a three Acousto-Optic-Modulator (AOM) . The first one is a double pass ( *Gooch & Housego -AOM AOMO 3200-124*) configuration with $230\,MHz$ on the $-1$ order. This configuration gave the ability to change the frequency without changing the optic system (Outgoing angle does not change when changing the frequency of the AOM). The second AOM ( *Gooch & Housego -AOM AOMO 3200-124*) has a frequency of $200\,MHz$ ($+1$ order) .

The relation between the $f_{lock}$ and $f_{co(1,2)\rightarrow 2}$ is:

$$f_{lock} \quad = \quad f_{co(1,2)\rightarrow 2} - \frac{f_{AOM-SAS}}{2} - f_{double-pass}$$

Therefore, the frequency shift is

$$
\begin{aligned}
\Delta f &= f_{cooling(f=9/2 \to f'=7/2)} - f_{lock} \\
&= 704.85 - 60 - 230 \times 2 \\
&= 202.55\ MHz
\end{aligned}
$$

We added the third AOM ( *Gooch & Housego -AOM AOMO 3200-124*) at $+200MHz$ for the final frequency transition. Prior to the third AOM we added a home made Tapered Amplifier (TA) to increase the laser power. The beam after the TA is diverging on an axis parallel to the table. Therefore we added a cylindrical lens with $f = 75mm$. After that we added a telescope 4:1 to get a small beam for the third AOM. We took the first positive order and made another telescope 1:2 to match the beam mode to the fiber mode.

For the repump laser, we used the cooling beam and added a sideband by using home-made high frequency Electro-Optic-Modulator (EOM 4.3.2). Then laser beam is injected to three optical fibers (the 3d MOT fibers)

The control of the power beam is done by changing the RF AOM power (with a voltage variable attenuator (*Mini circuits ZX73-2500-s+*)).

### 4.3.2 High Frequency Electro-Optic-Modulator

Cooling process requires two laser frequencies, one for cooling and one for repumping (3.1.2). In $^{40}K$ the $D_1$ transition has a distance of 1.285 $GHz$. Therefore, as in the MOT we can take two different lasers locked by an offset locking technique. However, in $D_1$ cooling, the frequency shift is the frequency shift between $|-9/2\rangle \to |-7/2\rangle$ in $^2S_{1/2}$. In addition, in $D_1$ cooling the magnetic field is set to zero and the states distances are not changed. Therefore, we can use an Electro-Optic-Modulator (EOM) to add frequency side band on the top of the cooling laser that are $\pm 1.285Ghz$ apart from the main laser frequency.

EOMs are based on the linear Electro-Optic effect, the modification of the refractive index of a non-linear crystal by electric field, in proportion to the field strength.
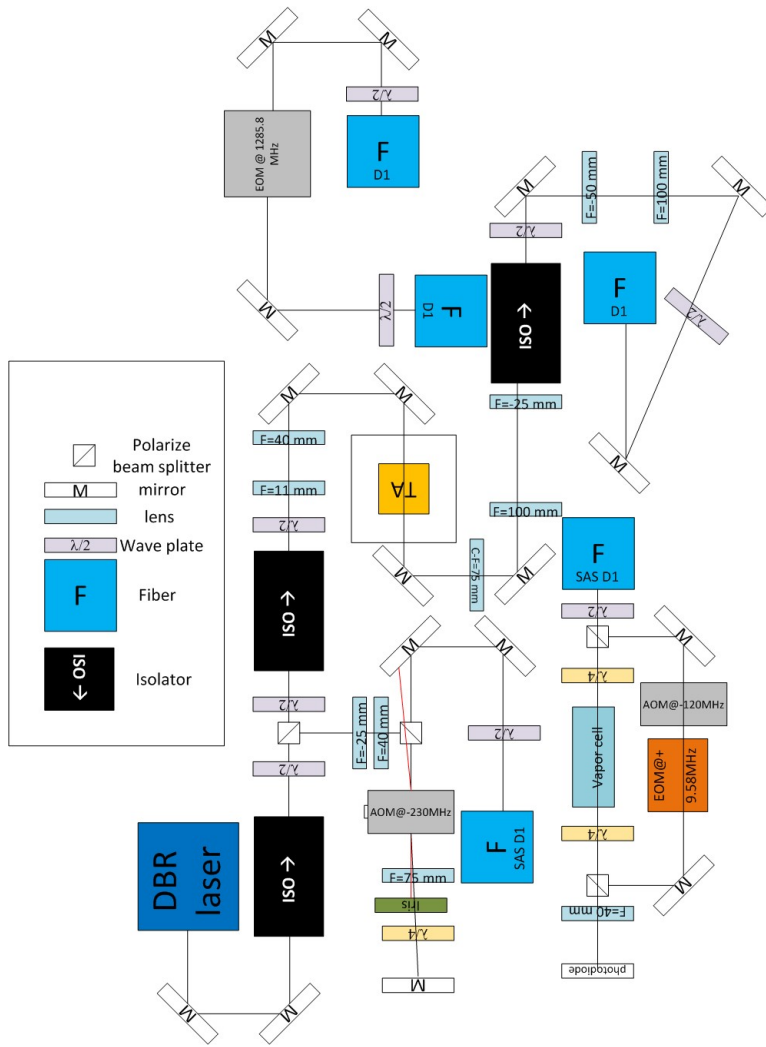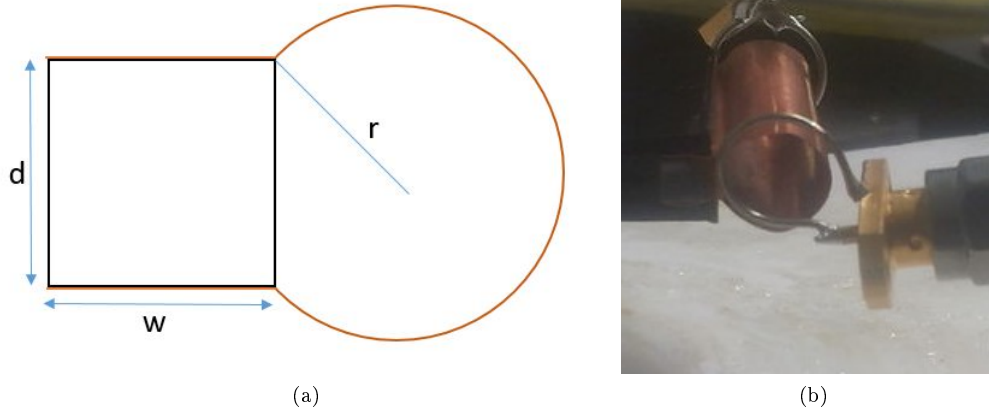
Figure 24: D1 laser setup.

Figure 25: a) High Frequency EOM prescription. The black square with area of $A = w * d$ is the crystal area cross section and the brown with radios r is the foil with a thickness of *0.1mm.* b) EOM picture where one loop is for antenna and anther is a pickup coil for Q factor measurement.

The electric field at $\omega_0$ enters into the medium where operates another electric field at $\omega_m$. So the equation of the field is

$$E(t) = E_0 \left( \sin \left( \omega_0 t + n \sin \left( \omega_m t \right) \right) \right)$$

$$= E_0 \sum_{n=0}^{\infty} J_n(n) \sin \left( \left( \omega_0 + n \omega_m \right) t \right)$$

This new phase can be applied by sending the electric field through a nonlinear crystal, resulting in a corresponding change in the refractive index. To make a significant change in the crystal there should be produced a high voltage with a frequency of $\omega_m$ on the crystal. There are electronics that can generate a high frequency voltage of more than $1GHz$. Therefore, we needed to produce a resonant circuit [44]. I constructed a circuit from copper foil with thickness of 0.1 mm . I made a loop with $3\ mm$ space for contact with the crystal ($LiNbO_3$) (fig 25).

The crystal could be described as an ideal capacitor. Therefore, $C = \epsilon wl/d$ , where $\epsilon$ is a dialectic constant at $\omega_m$. Also the accumulative inductance of the copper foil loop can be described as an ideal cylinder current sheet ( because $2\pi r \gg d$ ) $L = \mu_0 \pi r^2/l$. Therefore the resonant frequency of this $CL$

circuit is given as

$$f_0 = \frac{1}{2\pi} \left(\frac{c}{r}\right) \left(\frac{d}{\pi w \left(\epsilon_w/\epsilon_0\right)}\right)^{1/2}$$

We used a crystal of dimensions $w = d$ , and $c$ is speed of light. I calculated that in our experiment $(f_0 = 1.285 Ghz)$ $r \approx 4.15~mm$ (the value of $\epsilon_w$ at this frequency is not known and therefore we assume that it is $\sim 43$).

In our lab we used a $LiNbO_3$ crystal with dimensions of $3 \times 3 \times 30~mm$. If the crystal would have been smaller then 3 by 3 mm then the gap would have been smaller, resulting in a larger electric field for a given a power. However, the laser beam has to go through the crystal and our laser beam is a 1.5 $mm$, Therefore, a crystal with dimensions of $3 \times 3~mm$ is well suited to our lab.

I constructed the design for this EOM. The holder of the crystal is formed from Teflon, to prevent unwanted changes to the resonator quality (due to inductance).

Copper foil with a thickness of 0.1 $mm$ was polished in order to maximize the transmission of the foil. Then, I twisted the foil on a drill with a diameter of 8.3 $mm$. Both sides of the copper cylinder were bent, so that a surface of 3 $mm$ would fit the dimensions of the crystal.

I made a hole in the Teflon holder and threaded the RF antenna (end loop). For good coupling, we required that the antenna be located as close to the copper foil cylinder as possible, but it should not block the path of the optical crystal and not touch the foil. The antenna was connected to a Voltage Control Oscillator (*Mini Circuits ZX95-1410+*).

Next, I measured the quality of the resonator. The $Q$ (quality) factor describes how much energy
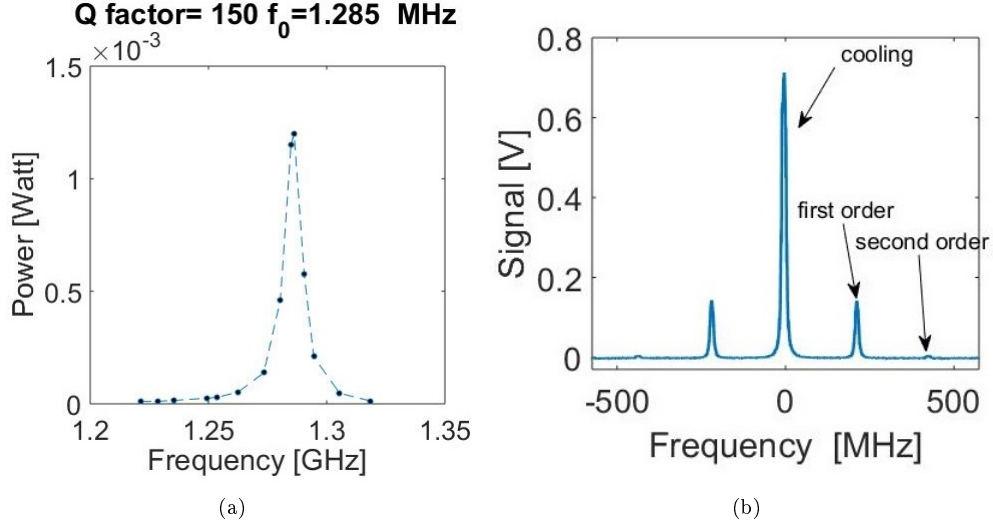
51

**Q factor= 150 f$_0$=1.285 MHz**

(a)                                    (b)

Figure 26: a) Measurement of Q factor $Q \approx 150$ and $f_0 = 1.285 \ GHz$ . b) Measurement of EOM efficiency using Fabry Perot. The maximum efficiency (at high Rf power ~ 4W) of the EOM is $\frac{I_{repump}}{I_{cooling}} = 0.19$. The Fabry perot scanning is 1.5 $GHz$ and the first order peak distance is $1500-216 = 1284 \ MHz$ (in this figure we see the sideband from the next peak where the distance between them is 1.5 $GHz$ ).

is lost in the resonator ,with a large $Q$ meaning less energy lost. The $Q$ factor is defined as

$$Q = \frac{f_0}{\Delta f}$$

where $\Delta f$ is the bandwidth (where the energy is reduced by half the maximum value) and $f_0$ is the resonance frequency.

I measured the $Q$ factor with an RF antenna and found that $Q \approx 150$ and $f_0 = 1.285 GHz$. This gave us the possibility of adjusting the device. The direction was made by a squeeze of the resonator, reducing the radius and thus increasing the resonant frequency.

In addition, we studied the effect on the laser by measuring the laser in a Fabry Perot. I took an RF power of $P = 4 W$ and got $\frac{I_{repump}}{I_{cooling}} = 7.5\%$ (fig. 26b) ,which should be sufficient for the $D_1$cooling.
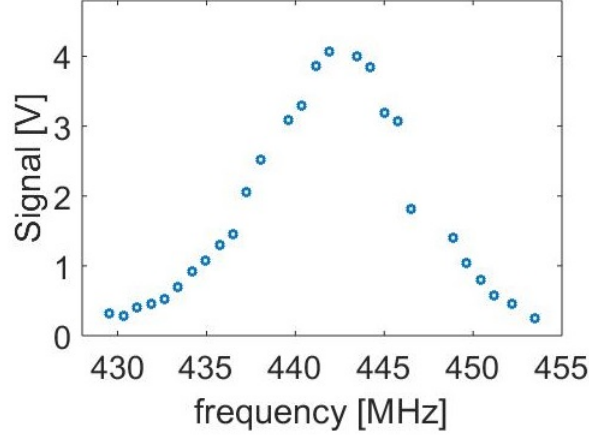
Figure 27: PMT signal Vs. DP-AOM frequency. The resonance is in $2 \cdot f_{AOM-DP} = 443 \, MHz$. To get the cooling with the blue detuning of $\sim 3\Gamma$ on the $D_1$ we need to add $18 \, MHz$ therefore, $2 \cdot f_{AOM-DP} = 461 \, MHz$. The final parameter will set by the atoms parameters (temperature and number of atoms) as shown in fig 28.

### 4.3.3 Measurement of the $D_1$ Frequency Resonance

In the first measurement we wanted to find the resonance frequency of the cooling transition $(|F = 9/2\rangle \rightarrow |F' = 7/2\rangle)$ . For this measurement, we used a Photo Multiplier Tube (PMT) to measure the fluorescence of the atoms. We opened the PMT $3 \, ms$ before opening the $D_1$ laser (just cooling) as the PMT has an opening time of $\sim 2 \, ms$. When we opened the cooling laser, the atoms are fluorescent for $\sim 100 \mu s$. Therefore, we see a signal of exponential decay. We made a fit of $I = A_0 e^{-t/\tau}$ and took the $A_0$ as the intensity of the atoms fluorescence. We scanned over a range of $f = 25 \, MHz$. We can not scan over more than $25 \, MHz$ as we scan on the double-pas AOM before the locking circuit and any change in this AOM changes the intensity on the locking signal and the laser would lock out. We found that the cooling resonance is at $f_{AOM-DP} = 221.175 \, MHz$ with a width of $10.02 \, MHz$. We set the cooling frequency with blue detuning at

$$f_{DP-AOM} = f_{resonance} + 3\Gamma = 233.675 \, MHz$$

Next we added the repump frequency to the cooling beam by using a High Frequency EOM. This laser has two frequencies which are injected to the 3 fiber of the 3d MOT (retro-reflection configuration). The power ,at each axis, is approximately $I = 12I_{sat}$ with $\frac{I_r}{I_c} \sim 7.5\%$. Before we start to reduce the temperature, we need to compress the atoms by adding a magnetic-trap for $2\ msec$ (which causes temperature increase).

### 4.3.4   Temperature and atoms number measurement by Time Of Flight (TOF ) technique

TOF measurements are performed by acquiring the absorption signal of the probe laser beam through the falling and expanding atomic cloud. There are several methods of measurement of temperature, R&R 4.2.6 , MOT fluorescence spectrum analysis[45],forced-oscillation[46]. Another model that was suggested by Jerzy and Gawlik in [47]shows that the absorb signal from an atoms

$$N\left(t\right) = \frac{P_0}{2\pi\left(\sigma_I^2 + \sigma_t^2\right)} \exp\left[-\left(\frac{g\left(t_0^2 - t^2\right)}{2\sqrt{2}\sqrt{\sigma_I^2 + \sigma_t^2}}\right)^2\right]$$

where $p_0$ is the probe laser power, $t_0$ is the arrival time of atoms with no initial vertical velocity, $\sigma_I$ are laser beam waist along $x$ and $y$ axes and $\sigma_t = \sqrt{\sigma_0^2 + \sigma_v^2 t^2}$ is the Gaussian radius of the ballistic expanded cloud. The Gaussian radius $\sigma_v$ of the velocity distribution is associated with the temperature $T$ of the atoms cloud by

$$T = \frac{m}{k_B}\sigma_v^2$$

After a loading time of $30\ sec$ we closed the coil current and the $D_2$ laser beam and opened the $D_1$cooling for $t = 4\ msec$. We then closed the $D_1$ laser, waited $18\ msec$ and then took a TOF image. I scanned the parameters of the cooling and repump frequency and optimized these parameters as describe in fig 28. At the end, the atoms parameters $T = 19\ \mu K$ and $N = 2 \times 10^8$atoms (where $f_{AOM-DP} = 461.3\ MHz$, $f_{repump} = 1287\ MHz$ and $D_1$ duration $t = 4\ msec$). The TOF image is shown in fig 28d.

(a)                                      (b)
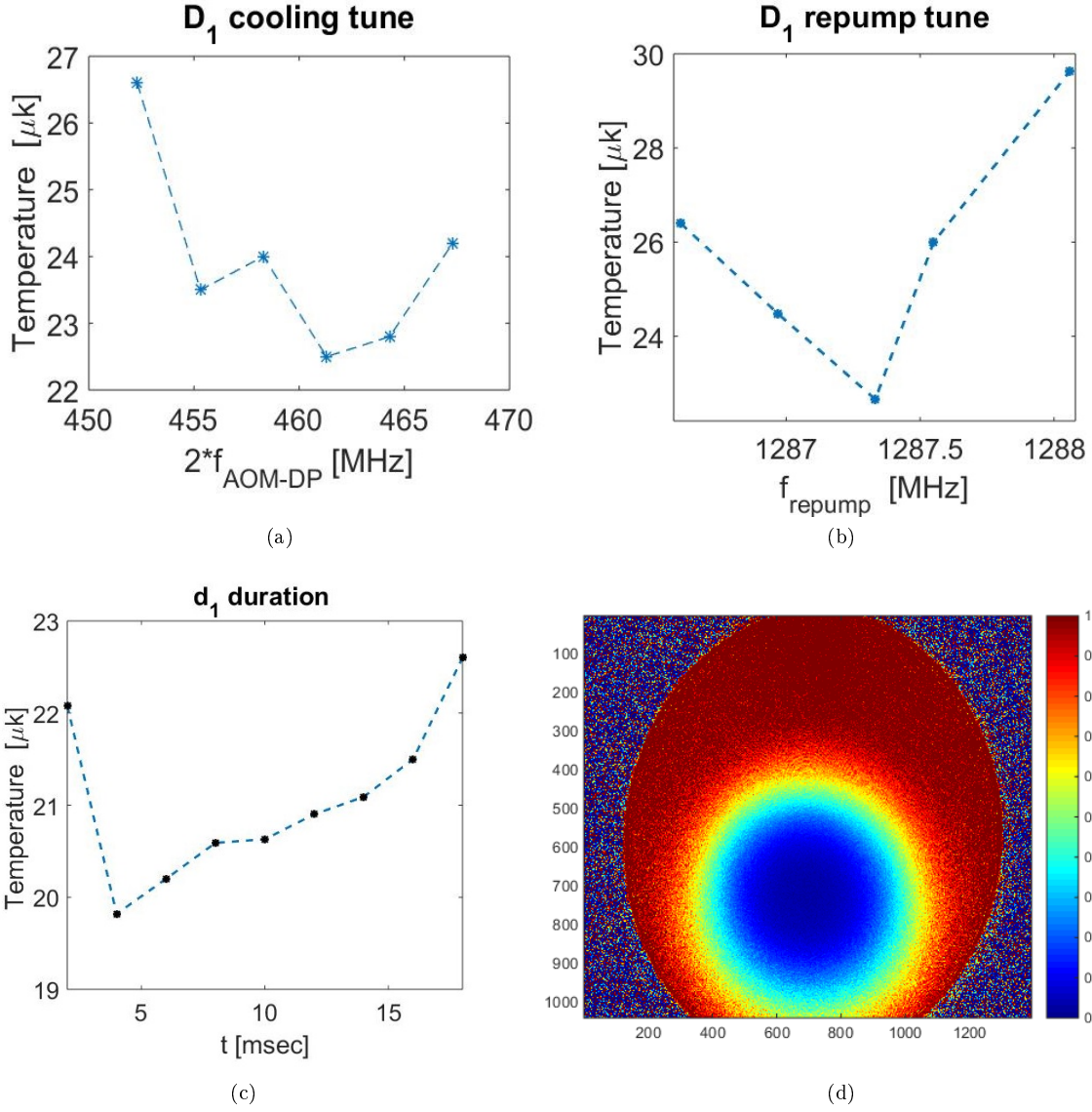




(c)                                      (d)

Figure 28: a) $D_1$cooling tune vs temperature. b) $D_1$ repump tune vs temperature. c) $D_1$ duration vs temperature d) Absorb image of atoms after $D_1$ cooling with Time Of Flight $t = 18 \ msec$

## 4.4   Optical Trap

As shown above (14), in a microtrap, the potential and the scattering rate depend on the beam $\omega_0$

$$U_{dip} \propto \omega_0^{-5}$$

Therefore we need precise measurement of the beam waist. In addition, we want to use a laser with $\lambda = 1064 \, nm$ in order to obtain a long lifetime in the micro trap (2) .

### 4.4.1   Microtrap waist measurement

In order to know the optical trap's depth and size, we need to measure the $\omega_0$ of the beam. Each camera has a finite size of the pixel which is greater than $7 \, \mu m$ so, we can not use a camera to measure the waist. We can use a knife edge measurement but again, we need a high resolution x-y-z stage ($< 0.3 \, \mu m$ for seven less measurements at the waist).

We used two nice and easy ways to measure the micro-trap waist.

A collimated laser beam with waist $\omega_1 = 0.89 \, mm$ and $\lambda = 1064 \, nm$ enters a 1:6 telescope. It then travels through an Aspheric lens with $f = 26 \, mm$. The Numerical Aperture (NA) is given by

$$NA = \frac{2 \cdot 6 \cdot \omega_1}{2f} = 0.205$$

The NA of a Gaussian laser beam is then reduced to its minimum spot size by

$$NA = \frac{\lambda}{\pi \omega_0}$$

where $\lambda$ is the laser wavelength (in our trap $\lambda = 1064 \, nm$) and $\omega_0$ is the laser beam waist at the focus. Therefore

$$\omega_{0,theory} = \frac{\lambda}{\pi \cdot NA} = 1.65 \, \mu m$$

### 4.4.2   Measurement of a microtrap waist with an optical chopper

An optical chopper is a spinning wheel with holes at a constant frequency. The holes are used as a knife for the knife edge measurement. I set a photodiode after the chopper and measured power vs. time on a digital scope. By knowing the frequency of the chopper and the distance between the laser and the center of the chopper, we can calculate the the velocity of the knife. Therefore we can

translate the time to distance.

### 4.4.3 Measurement of the microtrap waist with a piezoelectric actuator and michelson interferometer

In this measurement I inserted a Piezoelectric actuator ($Thorlabs\,AE0203D08F$) to a translation stage. In our labs we only have an actuator that can travel at $9.1\,\mu m$. The actuator receives a voltage of $0-150\,V$ from a ramp waveform. On the translation stage, I set a knife and measured the power on the photodiode. We can assume that the actuator travels linearly from $0 \rightarrow 9.1\;\mu m$, but we can calibrate this with a Michelson interferometer (calculate the actuator traveling distance) .As describe in fig (29a),I took our collimated laser $\lambda = 1064\,nm$ and split it with a Non Polarize Beam Splitter (NPBS) to two mirrors. One mirror is moved with the translation stage by the actuator and the second mirror does not move. The lasers from the two mirrors are combined on the NPBS and focused on a photodiode. On the photodiode we obtain a diffraction pattern that is dependent on the difference between the optical paths [?].

$$\Delta L = \frac{\lambda m}{2}$$

where $\Delta L$ is the distance that the mirror is moved, $m$ is the number of maximums and $\lambda$ is the wavelength of the laser. As shown in figure 29b we get $m = 14.5$ in one waveform period and therefore

$$\Delta L = 7.714\,\mu m$$

Now, I can calculate the distance in the knife edge measurement and I obtained $\omega_0 = 2.148 \mu m$ . With these measurements I can not know about aberration or about $M^2$. In order to measure them, there is a need to make measurements of $\omega(z)$, but for this, there is a need for a long travel Piezoelectric actuator $(\Delta L > 15 \cdot \omega_0).(30)$

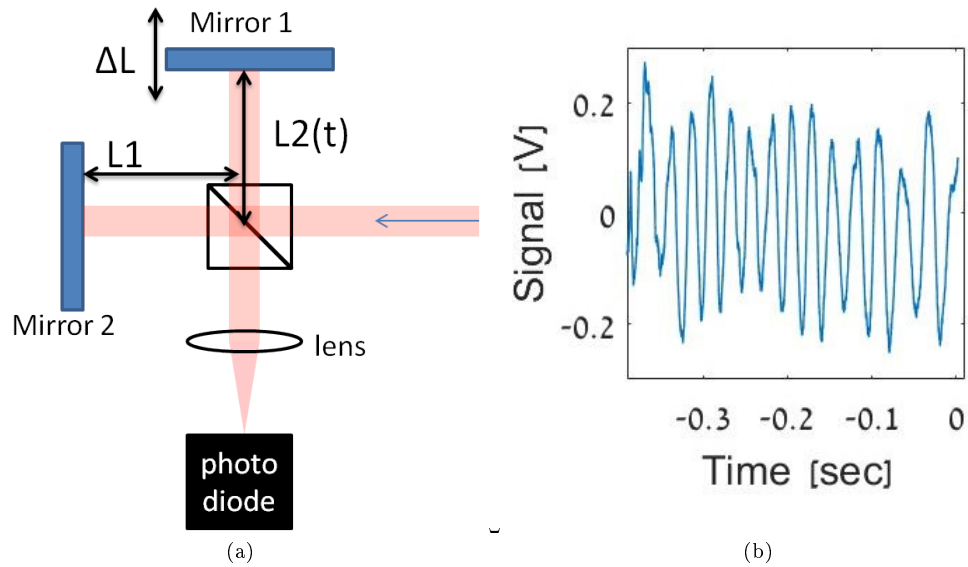(a)                                                                    (b)

Figure 29: Measuring the Microtrap Waist with a Piezoelectric Actuator and a Michelson Interferometer. a) The system description. Collimated laser beam splited by NPBS and go to two mirror (mirror 1 is on the translation state and mirror 2 is fixed). They reflected back and combined on the NPBS and focused on a photodiode. b) Interferometer result. We can see that we get 14.5 maximum peaks so the actuator travel is $7.714\,\mu m$. We also can see that the travel path of the piezo actuator is not linear (the frequency of the sin function is not the same).


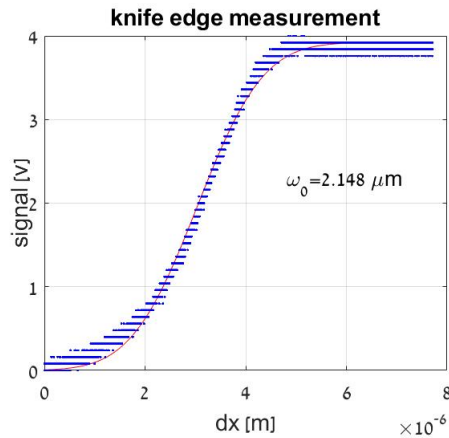
Figure 30: Calculation of the beam waist with Knife edge technique

# 5    Summery and Future Plan

In this study, I presented our new platform for quantum computation. It is based on fermion statistics and the attributes of ultracold atoms. In Chapter 1 I introduced the fundamentals of quantum computing and the features of ultracold atom.

In Chapter 2 we demonstrated the theory behind quantum computation solutions for our system. In addition, I explained the one qubit gates and two qubits gate in ultracold fermion systems. In addition, I presented our indecision regarding the choice of system form between the **Degenerate fermi gas system** (cooling to low temperature and then loading to a micro trap) or the **fast approach System** (loading to an optical microtrap and then cooling the atoms to ground state).

In Chapter 3 I give a relevant background for ultracold atoms and in Chapter 4 I described our two systems that are in the middle of construction. I show the MOT trapping and cooling stage and $D_1$ cooling with one laser.

Looking ahead in time, we need to carry out a more theoretical study on the system parameters such as the velocity $d(t)$ of one qubit without change the qubit state , defining $U$ and $t$ for a $\sqrt{SWAP}$ gate in order to obtain fidelity $\mathcal{F} = 1$, and more.
From an experimental point of view, we need to strive to reach a numbers of goals.

- Loading several atoms to a microtrap and developing the ability to measure a single atom.

- Reducing the number of atoms to one.

- Construction of two tunable microtraps with the application of a one and two qubit gate.

- Numerical calculation of the gates parameter ($U$, $t$, $d(t)$, trap parameter, etc.).

I hope that in a few years we will be able to provide answers to these and other issues.

# References

[1] R. P. Feynman, "Simulating physics with computers," *International journal of theoretical physics*, vol. 21, no. 6, pp. 467–488, 1982.

[2] P. W. Shor, "Algorithms for quantum computation: Discrete logarithms and factoring," in *Foundations of Computer Science, 1994 Proceedings., 35th Annual Symposium on*, pp. 124–134, IEEE, 1994.

[3] L. K. Grover, "Quantum mechanics helps in searching for a needle in a haystack," *Physical review letters*, vol. 79, no. 2, p. 325, 1997.

[4] J. I. Cirac and P. Zoller, "Quantum computations with cold trapped ions," *Physical review letters*, vol. 74, no. 20, p. 4091, 1995.

[5] J. P. Home, D. Hanneke, J. D. Jost, J. M. Amini, D. Leibfried, and D. J. Wineland, "Complete methods set for scalable ion trap quantum information processing," *Science*, vol. 325, no. 5945, pp. 1227–1230, 2009.

[6] J. L. O'Brien, "Optical quantum computing," *Science*, vol. 318, no. 5856, pp. 1567–1570, 2007.

[7] C. Weitenberg, S. Kuhr, K. Mølmer, and J. F. Sherson, "Quantum computation architecture using optical tweezers," *Physical Review A*, vol. 84, no. 3, p. 032322, 2011.

[8] A. Imamog, D. D. Awschalom, G. Burkard, D. P. DiVincenzo, D. Loss, M. Sherwin, A. Small, *et al.*, "Quantum information processing using quantum dot spins and cavity qed," *Physical Review Letters*, vol. 83, no. 20, p. 4204, 1999.

[9] R. Barends, J. Kelly, A. Megrant, A. Veitia, D. Sank, E. Jeffrey, T. C. White, J. Mutus, A. G. Fowler, B. Campbell, *et al.*, "Superconducting quantum circuits at the surface code threshold for fault tolerance," *Nature*, vol. 508, no. 7497, pp. 500–503, 2014.

[10] D. P. DiVincenzo *et al.*, "The physical implementation of quantum computation," *arXiv preprint quant-ph/0002077*, 2000.

[11] D. Loss and D. P. DiVincenzo, "Quantum computation with quantum dots," *Physical Review A*, vol. 57, no. 1, p. 120, 1998.

[12] M. A. Nielsen and I. L. Chuang, *Quantum computation and Quantum information.* Cambridge University Press India, 2000.

[13] L. W. Cheuk, M. A. Nichols, M. Okan, T. Gersdorf, V. V. Ramasesh, W. S. Bakr, T. Lompe, and M. W. Zwierlein, "Quantum-gas microscope for fermionic atoms," *Physical review letters*, vol. 114, no. 19, p. 193001, 2015.

[14] G. Edge, R. Anderson, D. Jervis, D. McKay, R. Day, S. Trotzky, and J. Thywissen, "Imaging and addressing of individual fermionic atoms in an optical lattice," *Physical Review A*, vol. 92, no. 6, p. 063406, 2015.

[15] Y. H. Fung, P. Sompet, and M. F. Andersen, "Single atoms preparation using light-assisted collisions," *Technologies*, vol. 4, no. 1, p. 4, 2016.

[16] A. M. Kaufman, B. J. Lester, and C. A. Regal, "Cooling a single atom in an optical tweezer to its quantum ground state," *Physical Review X*, vol. 2, no. 4, p. 041014, 2012.

[17] F. Serwane, G. Zürn, T. Lompe, T. Ottenstein, A. Wenz, and S. Jochim, "Deterministic preparation of a tunable few-fermion system," *Science*, vol. 332, no. 6027, pp. 336–338, 2011.

[18] C. Regal and D. Jin, "Experimental realization of bcs-bec crossover physics with a fermi gas of atoms," *arXiv preprint cond-mat/0601054*, 2006.

[19] L. Allen and J. E. O. Resonance, "Two-level atoms dover publications inc," *New York*, 1987.

[20] S. Kuhr *et al.*, *A controlled quantum system of individual neutral atoms.* PhD thesis, Universitäts- und Landesbibliothek Bonn, 2003.

[21] C. Chin, R. Grimm, P. Julienne, and E. Tiesinga, "Feshbach resonances in ultracold gases," *Reviews of Modern Physics*, vol. 82, no. 2, p. 1225, 2010.

[22] D. Hayes, P. S. Julienne, and I. H. Deutsch, "Quantum logic via the exchange blockade in ultracold collisions," *Physical review letters*, vol. 98, no. 7, p. 070501, 2007.

[23] J. Hubbard, "Electron correlations in narrow energy bands," in *Proceedings of the Royal Society of London A: Mathematical, Physical and Engineering Sciences*, vol. 276, pp. 238–257, The Royal Society, 1963.

[24] T. Esslinger, "Fermi-hubbard physics with atoms in an optical lattice," *Annu. Rev. Condens. Matter Phys.*, vol. 1, no. 1, pp. 129–152, 2010.

[25] C. Monroe, D. Meekhof, B. King, S. Jefferts, W. Itano, D. Wineland, and P. Gould, "Resolved-sideband raman cooling of a bound atom to the 3d zero-point energy," *Physical Review Letters*, vol. 75, no. 22, p. 4011, 1995.

[26] B. J. Lester, N. Luick, A. M. Kaufman, C. M. Reynolds, and C. A. Regal, "Rapid production of uniformly filled arrays of neutral atoms," *Physical review letters*, vol. 115, no. 7, p. 073003, 2015.

[27] H. R. Lewis Jr and W. Riesenfeld, "An exact quantum theory of the time-dependent harmonic oscillator and of a charged particle in a time-dependent electromagnetic field," *Journal of Mathematical Physics*, vol. 10, no. 8, pp. 1458–1473, 1969.

[28] D. J. Wineland, R. E. Drullinger, and F. L. Walls, "Radiation-pressure cooling of bound resonant absorbers," *Physical Review Letters*, vol. 40, no. 25, p. 1639, 1978.

[29] J. Dalibard and C. Cohen-Tannoudji, "Laser cooling below the doppler limit by polarization gradients: simple theoretical models," *JOSA B*, vol. 6, no. 11, pp. 2023–2045, 1989.

[30] M. Landini, S. Roy, L. Carcagní, D. Trypogeorgos, M. Fattori, M. Inguscio, and G. Modugno, "Sub-doppler laser cooling of potassium atoms," *Physical Review A*, vol. 84, no. 4, p. 043432, 2011.

[31] G. Modugno, C. Benkő, P. Hannaford, G. Roati, and M. Inguscio, "Sub-doppler laser cooling of fermionic 40 k atoms," *Physical Review A*, vol. 60, no. 5, p. R3373, 1999.

[32] D. R. Fernandes, F. Sievers, N. Kretzschmar, S. Wu, C. Salomon, and F. Chevy, "Sub-doppler laser cooling of fermionic 40k atoms in three-dimensional gray optical molasses," *EPL (Europhysics Letters)*, vol. 100, no. 6, p. 63001, 2012.

[33] H. J. Metcalf and P. van der Straten, "Laser cooling and trapping of atoms," *JOSA B*, vol. 20, no. 5, pp. 887–908, 2003.

[34] V. Letokhov, V. Minogin, and B. Pavlik, "Cooling and capture of atoms and molecules by a resonant light field," *Soviet Journal of Experimental and Theoretical Physics*, vol. 45, p. 698, 1977.

[35] E. Arimondo and G. Orriols, "Nonabsorbing atomic coherences by coherent two-photon transitions in a three-level optical pumping," *Lettere Al Nuovo Cimento (1971-1985)*, vol. 17, no. 10, pp. 333–338, 1976.

[36] J. A. Christensen and R. F. Squires, "4-phenylpiperidine compounds," Feb. 8 1977. US Patent 4,007,196.

[37] T. Esslinger, I. Bloch, and T. W. Hänsch, "Bose-einstein condensation in a quadrupole-ioffe-configuration trap," *Physical Review A*, vol. 58, no. 4, p. R2664, 1998.

[38] R. Grimm, M. Weidemüller, and Y. B. Ovchinnikov, "Optical dipole traps for neutral atoms," *Advances in atomic, molecular, and optical physics*, vol. 42, pp. 95–170, 2000.

[39] K. Dieckmann, R. Spreeuw, M. Weidemüller, and J. Walraven, "Two-dimensional magneto-optical trap as a source of slow atoms," *Physical Review A*, vol. 58, no. 5, p. 3891, 1998.

[40] U. Schünemann, H. Engler, R. Grimm, M. Weidemüller, and M. Zielonkowski, "Simple scheme for tunable frequency offset locking of two lasers," *Review of Scientific Instruments*, vol. 70, no. 1, pp. 242–243, 1999.

[41] T. Tiecke, "Properties of potassium," *University of Amsterdam, The Netherlands, Thesis*, pp. 12–14, 2010.

[42] R. S. Williamson III, *Magneto-optical trapping of potassium isotopes*. PhD thesis, UNIVERSITY OF WISCONSIN–MADISON, 1997.

[43] D. S. Weiss, E. Riis, Y. Shevy, P. J. Ungar, and S. Chu, "Optical molasses and multilevel atoms: experiment," *JOSA B*, vol. 6, no. 11, pp. 2072–2083, 1989.

[44] J. Kelly and A. Gallagher, "Efficient electro-optic modulator for optical pumping of na beams," *Review of scientific instruments*, vol. 58, no. 4, pp. 563–566, 1987.

[45] C. Westbrook, R. Watts, C. Tanner, S. Rolston, W. Phillips, P. Lett, and P. Gould, "Localization of atoms in a three-dimensional standing wave," *Physical review letters*, vol. 65, no. 1, p. 33, 1990.

[46] P. Kohns, P. Buch, W. Süptitz, C. Csambal, and W. Ertmer, "On-line measurement of sub-doppler temperatures in a rb magneto-optical trap-by-trap centre oscillations," *EPL (Europhysics Letters)*, vol. 22, no. 7, p. 517, 1993.

[47] T. M. Brzozowski, M. Maczynska, M. Zawada, J. Zachorowski, and W. Gawlik, "Time-of-flight measurement of the temperature of cold atoms for short trap-probe beam distances," *Journal of Optics B: Quantum and Semiclassical Optics*, vol. 4, no. 1, p. 62, 2002.